scientific reports

Check for updates

OPEN

Hierarchical climate-driven dynamics of the active channel length in temporary streams

Gianluca Botter[1]✉, Filippo Vingiani[1], Alfonso Senatore[2], Carrie Jensen[3], Markus Weiler[4], Kevin McGuire[3], Giuseppe Mendicino[2] & Nicola Durighetto[1]

Looking across a landscape, river networks appear deceptively static. However, flowing streams expand and contract following ever-changing hydrological conditions of the surrounding environment. Despite the ecological and biogeochemical value of rivers with discontinuous flow, deciphering the temporary nature of streams and quantifying their extent remains challenging. Using a unique observational dataset spanning diverse geomorphoclimatic settings, we demonstrate the existence of a general hierarchical structuring of river network dynamics. Specifically, temporary stream activation follows a fixed and repeatable sequence, in which the least persistent sections activate only when the most persistent ones are already flowing. This hierarchical phenomenon not only facilitates monitoring activities, but enables the development of a general mathematical framework that elucidates how climate drives temporal variations in the active stream length. As the climate gets drier, the average fraction of the flowing network decreases while its relative variability increases. Our study provides a novel conceptual basis for characterizing temporary streams and quantifying their ecological and biogeochemical impacts.

River networks shape the Earth landscape transporting water and sediments from the uplands to the sea, and provide a number of invaluable ecosystem services [e.g.][1,2]. For decades, the spatial organization of streams has stimulated scientific debate around observed morphological and ecological patterns in river basins. At fine scales, the location of the channel heads has been the focus of pioneering work[3,4] that fuelled an array of methodologies for the analysis of Digital Terrain Maps; at larger spatial scales, theoretical investigations examined origins and implications of the branching shape of river networks and their fractal nature[5–10]. Recently, the temporal dimension of river networks has been recognized as a core issue not only over geological timescales typical of landscape evolution models, but also during individual years or seasons, within which river segments may temporarily cease to flow [e.g.][11–13]. This empirical evidence has shown that the active portion of channel networks experiences a continuous sequence of expansion and contraction cycles driven by precipitation. Temporary streams, here defined as fluvial systems that periodically cease to flow, are observed in a wide range of climatic settings and represent an important fraction of global rivers[11,14]. The study of active stream dynamics is pivotal not only to characterize spatial patterns of hydrologic regimes but also to understand the influence of flow intermittency on e.g. ecological dispersion, in-stream processes, hyporheic exchange and nutrient spiraling[15–20].

Growing empirical efforts in monitoring network dynamics have also provided enhanced insight into the underlying driving processes. In particular, recent work has suggested that the transitions between dry and wet channels are governed by the local imbalance between the capacity to transmit flow in the subsurface and the seepage flow delivered from upslope—usually conceived as proportional to the local contributing area[12,21]. As the local transmissivity and the contributing area may be durable features of a landscape, this conceptual scheme may also suggest the existence of a hierarchy in the activation of different branches of temporary streams as a function of the underlying catchment wetness. However, the activation order of different reaches of a dynamic stream network has never been quantitatively explored in the literature, and the potential implications for the dynamics of the active drainage density under diverse hydroclimatic conditions have not been disclosed. Furthermore, a comparative analysis of stream length variability across different climatic regimes is lacking.

[1]Department of Civil, Environmental and Architectural Engineering, University of Padua, Via Marzolo 9, 35131 Padua, PD, Italy. [2]Department of Environmental Engineering, University of Calabria, Via Pietro Bucci 42, 87036 Arcavacata di Rende, CS, Italy. [3]Department of Forest Resources and Environmental Conservation, Virginia Tech, Cheatham Hall, 210B, 310 West Campus Drive, Blacksburg, VA 24061, USA. [4]Fakultät für Umwelt und Natürliche Ressourcen, Universität Freiburg, Friedrichstr. 39, 79098 Freiburg, Germany. ✉email: gianluca.botter@dicea.unipd.it

Here a combination of theoretical analysis and empirical observations is used to address the following questions:

- Is there a mathematical relationship between the activation or deactivation order of different reaches of a dynamic network and the corresponding degree of flow persistency of those reaches? And what are the implications in terms of network spatial correlation and temporal changes of active length?
- Can we identify constraints in the temporal variations of the active drainage density that incorporate the complex effect of climate?

Due to the unique contribution of temporary streams to biodiversity and nutrient cycling [e.g.][22,23], these issues are becoming urgent for identifying sustainable water management strategies and assessing the full ecological and biogeochemical function of drainage networks[19,24–26].

The basic hypothesis of this work is that the local persistency of different river stretches of a stream network (i.e. the percentage of time during which water is flowing over different locations of a watercourse) defines their activation and deactivation order during individual storm events and across seasons. We also postulate that the mean persistency of the entire network represents the primary link between the temporal variability of active stream length and the underlying climatic drivers. While intuitive, these hypotheses have never been formally assessed in the existing literature and—most importantly—their implications in terms of active length dynamics have not been disclosed. Here, the proposed research hypotheses were tested analyzing seasonal (or annual) event-based dynamics of the active network in 19 European and North-American catchments (Fig. 1a), encompassing a broad range of climatic conditions, land-cover, drainage areas and geology.

Hierarchical activation of temporary streams

For each study site, flow presence maps representing the observed active network on different dates were produced using multi-month field mapping campaigns (with a mean frequency of two weeks) or water presence sensors (with a sub-hourly resolution). These maps were converted into sets of geo-referenced nodes with binary states (wet/dry), and the local persistency of each node (P_i) was calculated as the relative fraction of data indicating the presence of flowing water in that location. Afterwards, each flow presence map was compared with the outcome of a hierarchical model in which the network nodes were switched on from the most to the least persistent, until the total number of nodes observed as active during the corresponding survey was reached (Methods). Regardless of the underlying climatic and geologic complexity, the accuracy of the hierarchical model (here defined as the relative number of nodes properly classified as wet or dry throughout a river network during all the surveys) typically exceeded 99% (Fig. 1b), with a minimum accuracy around 95% for two European rivers, the Attert and the Valfredda (Fig. 1c). The average accuracy is very high, and much higher than the accuracy of a random model that assigns the status of each node at random independently on the status of the other nodes but consistently with the local persistency, which is $0.79 \pm 0.075\%$ for our selection of case studies (SI). Thus, our observations suggest that the most persistent nodes were generally the first to activate during individual rainfall events and the last to dry-out during the subsequent recessions. The less persistent nodes, instead, were mostly switched on only in response to the most significant rain events and when all the nodes with a higher persistency were already active. This behaviour is aligned with that foreseen by the conceptual model proposed by[12,21], based on a set of physical assumptions which are not required by the purely statistical approach developed in this paper.

The most common exceptions to the hierarchical behaviour observed in our set of case studies were the following: (1) nodes with a relatively low persitency that activate in the early stage of a rain event (Poverty Creek); (2) lack of symmetry in the rate and/or the direction of wetting and drying processes (Valfredda, Turbolo); (3) inter-event shifts in the wetting mechanism (e.g. from the downstream propagation of a saturation front induced by intense events taking place after dry periods to the upstream expansion of saturated areas around the permanent network, as observed in the Valfredda). In spite of this complexity, the hierarchical phenomenon was dominant across the full range of climatic conditions, temporal resolutions and spatial scales explored in the paper. In particular, the hierarchical activation rule applied also to disconnected river networks, where the nodes with the same persistency are not necessarily adjacent because of local discontinuities of landscape and geology (see Fig. 1c). This means that the hierarchical phenomenon is much more than a simple upstream/downstream propagation of a saturation front along the network[12]. In particular, our results indicate that stream sections potentially quite distant in the physical space (up to tens or hundreds of kilometers) might share the same average degree of persistency and exhibit systematically synchronous dynamics. Furthermore, the hierarchical scheme held also within catchments as large as several hundreds of km^2 (the Attert and the Seugne). These basins are characterized by significant internal landscape and climatic gradients that are potentially responsible for the unsystematic, selective activation of limited and specific portions of the river network. The ability of the hierarchical model to describe active stream dynamics in these larger river basins indicates that meso-scale channel network dynamics maximize the spatial correlation of the nodes' states (see Methods) and reflect a homogeneous signal, such as the total catchment storage, driven by mid-range antecedent precipitation (e.g. weekly to monthly rainfall, see[27]). Interestingly, the spatial homogeneity of the hydrological signal underpinning the hierarchical dynamics of temporary streams promotes the synchronization of node status within a channel network, regardless of the observed complex patterns of local persistency produced by spatially heterogeneous physiographic and morphometric features (see Fig. 1c and[28]).

The results shown in Fig. 1 bear important practical and theoretical implications. For instance, the hierarchical behaviour of temporary streams can streamline empirical surveys of river network dynamics, with beneficial consequences on the ability to characterize spatiotemporal patterns of flow persistency[29,30]. In perfectly hierarchical networks, the adoption of ad-hoc monitoring strategies that exploit information available from previous surveys

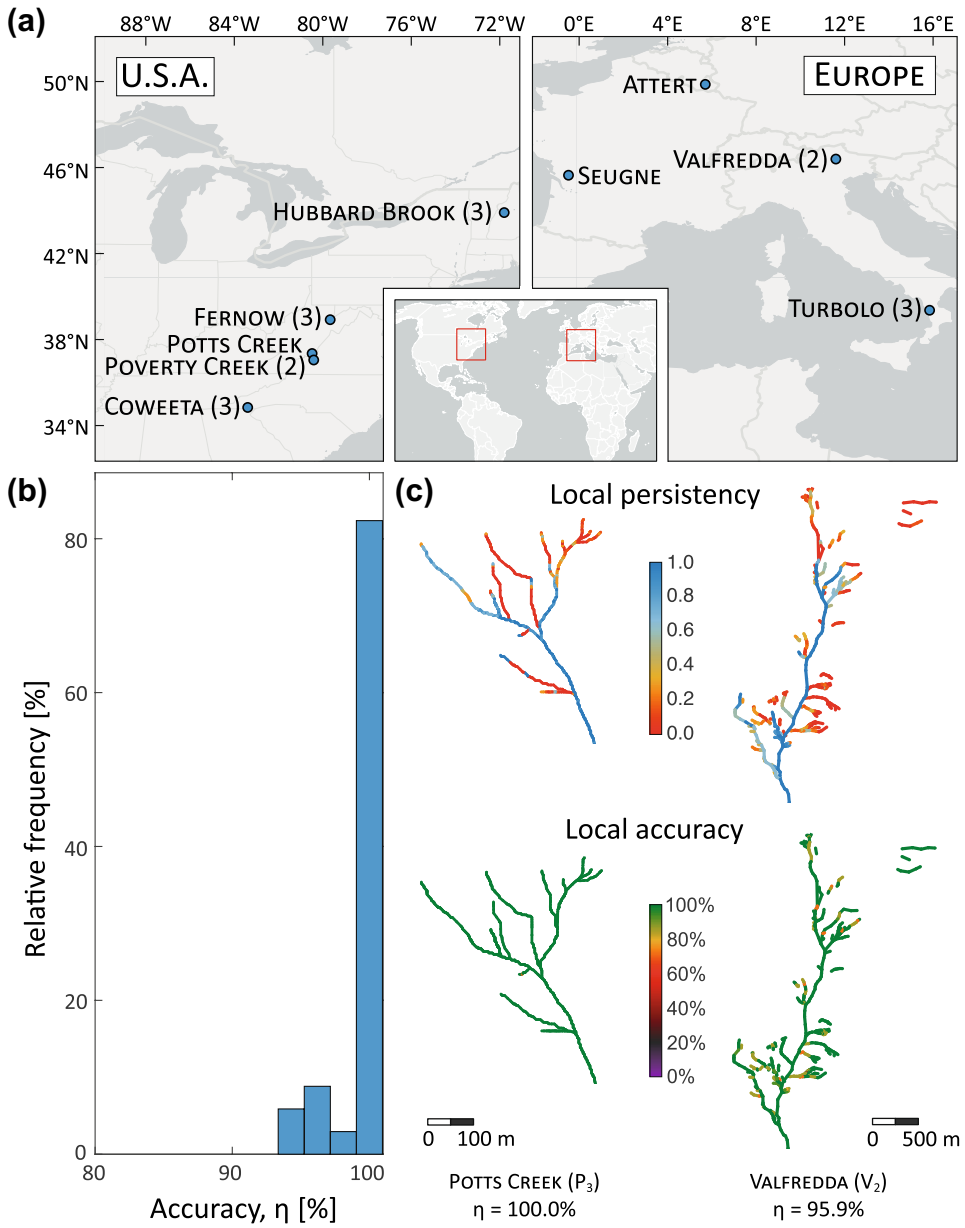

Figure 1. Study sites and performance of the hierarchical model, in which the activation (deactivation) of the nodes follows a strictly decreasing (increasing) order of persistency. (**a**) Geographical location of the study catchments across Europe and eastern USA. The number of case studies for each location is indicated within round brackets only when this number is larger than one. Map generated with Arcgis Pro 2.7.1 (www.arcgis.com). The histogram in (**b**) represents the relative frequency of the accuracy of the hierarchical model (relative number of nodes properly classified as wet or dry by the hierarchical model) for all the study catchments. The maps in (**c**) show spatial patterns of local persistency and local accuracy of the hierarchical model in the best and the worst cases (respectively South Fork of Potts Creek, USA and Valfredda Creek, Italy). Analogous maps for all the study sites are reported in Figures S2 and S5 of the Supplementary Information. For comparison, the corresponding maps of local accuracy obtained from the random model are represented in Figure S6.

can reduce the number of nodes to monitor during a long-term field campaign with at least 10 surveys by 40 to 75%, depending on the exact number of surveys and the mean network persistency (Supplementary Information). Although several initial surveys that include most of the network are needed to establish the hierarchy among the nodes, the saving in terms of number of surveys becomes particularly significant when the number of surveys exceeds 20—as typically needed to capture event-based variations of the active length, see Table 1 in[31]. This indicates that the hierarchical nature of stream dynamics could significantly facilitate the observational mapping of flowing streams in a broad range of settings, especially in large river basins. Furthermore, the existence of a fixed hierarchical order in the expansion and retraction of temporary rivers allows the identification of a one-to-one relationship between the total length of flowing streams and the spatial distribution of active nodes

in the network, if a spatial map of the local persistency is known e.g. based on multiple field surveys. This could help the reconstruction and the modeling of channel network dynamics, especially in cases where active length statistics can be indirectly inferred from rainfall and/or discharge observations[12,27,28,32].

Quantifying the mean active drainage density and its temporal variations

The observed hierarchical behaviour of river networks enabled the derivation of novel theoretical results that advance our ability to predict the dynamics of flowing channels in temporary streams. In hierarchical networks, in fact, active channel length statistics can be expressed analytically in terms of the mean network persistency, unveiling the complex linkage between climate and stream dynamics.

A river network was described by N nodes with a random binary state (wet/dry). The status of each node represents the hydrologic conditions of the portion of network that is associated to that specific node. To avoid the issue of identifying the status of a link connecting two neighbouring nodes with different states (wet/dry), the reach associated to the node i ($i \in (1, N)$) is not a link with one of the adjacent nodes but rather a stretch embedding the node i (Methods). Shifts in the status of the nodes produce changes in the flowing stream length, which are here characterized by the temporal variations of the active drainage density, D (defined as the active stream length normalized with the corresponding catchment area,[33]). In this framework, the average drainage density, $\bar{D}$, can be expressed as (Methods):

$$\bar{D} = \bar{P} D_g \,, \tag{1}$$

where $\bar{P}$ is the mean node persistency throughout the entire network ($\bar{P} = \sum_{i=1}^{N} P_i/N$ in case of equally spaced nodes) and D_g is the potential geomorphic drainage density, that corresponds to the simultaneous activation of all the N nodes in the channelized network, including streams that are typically dry but excluding what is out of the geomorphically obvious channel features and the hillslopes (where surface flow could be temporarily observed). When the activation of the nodes is hierarchical, the temporal coefficient of variation of the active drainage density, CV_D (that also corresponds to the temporal coefficient of variation of the active network length, CV_L) can be written as (Methods):

$$CV_D = CV_L = \sqrt{\frac{\bar{P}(1-\bar{P}) + \widetilde{\Delta P}}{\bar{P}^2}} \,, \tag{2}$$

where the term $\widetilde{\Delta P} = 2/N^2 \cdot \sum_{i=1}^{N} i(P_i - \bar{P}) \leq 0$ represents a weighted spatial average of the persistency deviations around the mean. Thus, $\widetilde{\Delta P}$ reflects spatial variation of persistency likely induced by patterns of geologic and morphometric attributes in the channel network or landscape.

Equation (2) allows for the identification of two distinct contributions to the temporal changes of the drainage density: a positive contribution proportional to $\bar{P}(1-\bar{P})$, determined by the mean persistency of the whole stream network, and a negative contribution proportional to $\widetilde{\Delta P}$, that depends on the internal spatial variability of P. Thus, an upper limit for the coefficient of variation of the active drainage density can be identified by setting $\widetilde{\Delta P} = 0$ in Eq. (2):

$$CV_D^{max} = CV_L^{max} = \sqrt{\frac{1-\bar{P}}{\bar{P}}} \,. \tag{3}$$

Equation (3) corresponds to the theoretical coefficient of variation of a homogeneous network made up of synchronous nodes sharing the same persistency ($\bar{P}$). In realistic cases, instead, the actual value of CV_D is influenced by the spatial variations of the local persistency. Enhanced internal geological, landscape and hydrological heterogeneities entail the spatial changes of flow persistence and increase $|\widetilde{\Delta P}|$, thereby reducing the variability of the active length. An emblematic example of this trend is represented by the catchments H_2 (Hubbard Brook, USA) and V_1 (Valfredda, Italian Alps). These are two case studies with a different degree of landscape heterogeneity that share the same mean persistency ($\bar{P} \simeq 0.6$). As predicted by Eq. (2), the observed value of CV_D in V_1, whose contributing catchment is characterized by five distinct lithological types and four diverse land uses[27], is approximately 40% lower than that of H_2, where vegetation and geology are more homogeneous in comparison[28].

To describe the influence of the spatial variability of the local persistency on CV_D, we developed an analytical model, in which a one-parameter beta probability density function was used to represent the heterogeneity of the persistency among the different nodes in the network. This led to the following equation for CV_D (Methods):

$$CV_D = CV_L = \sqrt{\frac{(1-\bar{P})^2}{\bar{P}(2-\bar{P})}} \,. \tag{4}$$

Differently from Eqs. (3), (4) accounts for the statistical distribution of flow intermittency within the river network. The resulting expression for CV_D, however, only depends on the mean network persistency because the term $\widetilde{\Delta P}$ of Eq. (2) was in turn expressed as a function of $\bar{P}$. The existence of a general link between $\widetilde{\Delta P}$ and $\bar{P}$ should not be surprising, since in perennial (or persistently dry) rivers all the nodes necessarily exhibit very similar persistencies—thereby implying that $\widetilde{\Delta P} \simeq 0$ for very high or very low values of $\bar{P}$.

The theoretical relationships between the statistics of the dynamic drainage density and the mean network persistency were tested using active length data derived from field surveys in our case studies (Fig. 2). As expected, the mean network persistency $\bar{P}$ well approximates the temporal average of the active drainage density normalized by the geomorphic drainage density, as implied by Eq. (1) (Fig. 2a). The 1:1 relationship between

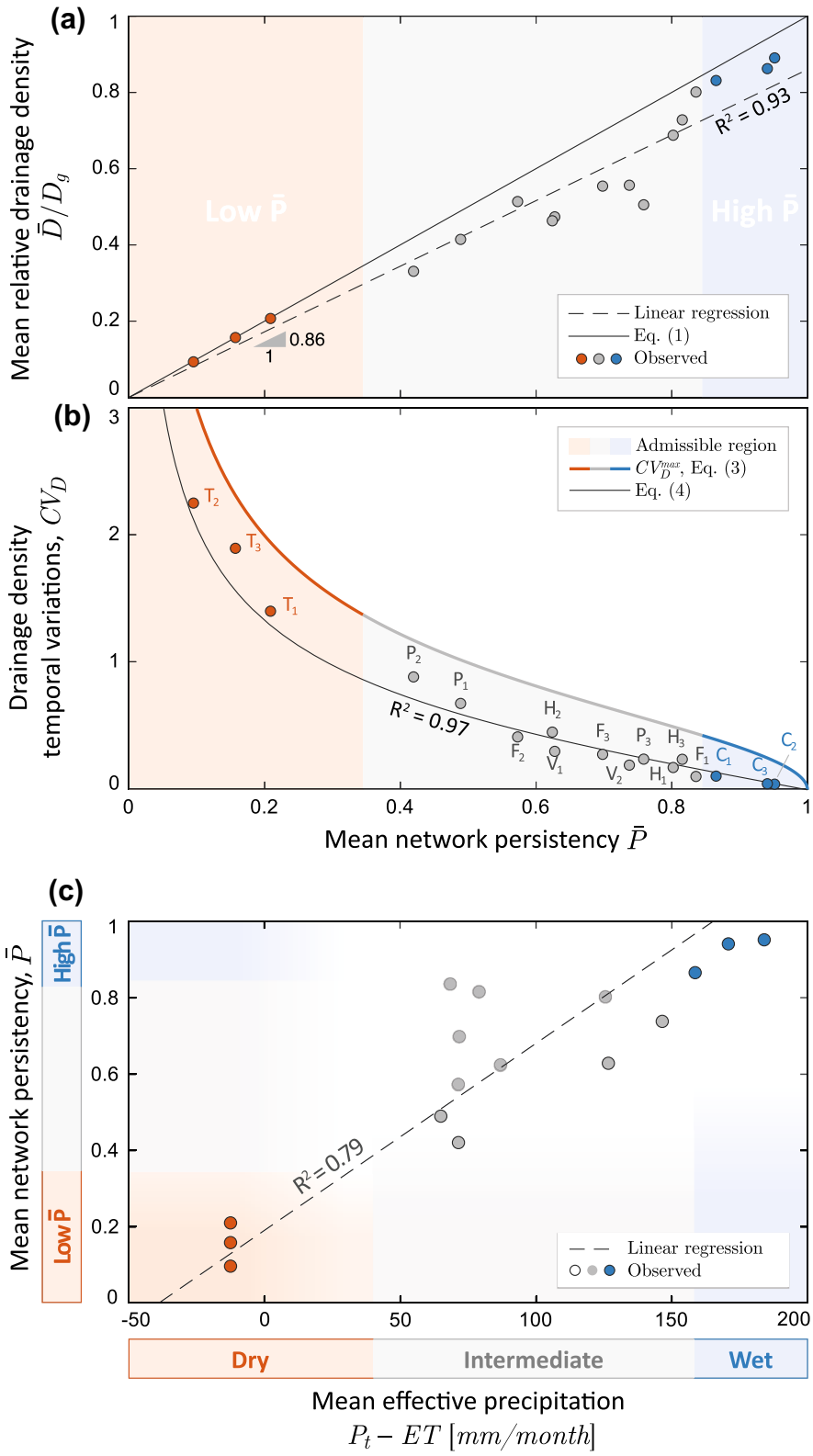

Figure 2. Climatic controls on the active drainage density. (**a**) mean drainage density scaled to the geomorphic drainage density as a function of the mean network persistency, $\bar{P}$; (**b**) coefficient of variation of the drainage density as a function of the mean network persistency $\bar{P}$. Also shown here are the maximum theoretical limit for CV_D (Eq. (3)) and the value of CV_D predicted by the hierarchical beta-model (Eq. (4)); (**c**) the correlation between mean network persistency and effective precipitation (total precipitation minus potential evapotranspiration ET) during the period when the active network was surveyed (average monthly value among all the months during which at least one field survey was performed). Points with a lighter gray border represent cases in which the surveys are not evenly distributed within the study period (Hubbard Brook and Fernow) as the median time between all the possible pairs of survey dates, τ_m, was smaller than 15 days. P_3 was not included in this plot because of the lack of reliable precipitation data.

the spatial average of the mean percentage of time during which a node is active and the temporal average of the normalized mean active length is implied by the linearity of the average operation. Because a 1:1 relationship between $\bar{P}$ and $\bar{D}/D_g$ is obtained regardless of the specific activation order that underlies the network dynamics, Fig. 2a should not be interpreted as a validation of the hierarchical scheme. The scattering of the points is only due to the fact that the geomorphic drainage density was calculated independently from the number of network surveys based on geomorphic signatures of the landscape (SI). Available data also confirm that the magnitude of CV_D is modulated by the mean network persistency across the entire set of study catchments, with higher values of CV_D and an enhanced sensitivity to $\bar{P}$ for low network persistencies (Fig. 2b). Remarkably, the analytical model given by Eq. (4) captures the observed network length variability across the full set of study catchments ($R^2 = 0.97$), proving that the temporal variation of active streams are in fact linked to the mean persistency of the river network. All the experimental points obey to the inequality $CV_D < CV_D^{max}$, indicating that the observed temporal dynamics of active stream length are properly constrained by the theoretical limit given by Eq. (3). This finite universal limit of the active length standard deviation derives from the contrasting patterns of $CV_D^{max}(\bar{P})$ and $\bar{D}(\bar{P})$ shown in Fig. 2 (Supplementary Information). The relatively small distance of the experimental points from the theoretical limit given by Eq. (3) suggests that the total active stream length is about as dynamic as it can possibly be (i.e., the CV of network length or drainage density is not far from its maximum possible value). Active stream dynamics and temporarily-dry channels are known to modify the distribution of catchment travel times owing to changes in the length of channel and hillslope flowpaths[27,34], thereby affecting important biogeochemical and ecological properties of rivers across a broad range of hydroclimatic settings[22,35–37]. Thus, temporal variations of the active channel length should be properly taken into account in regional assessments of biogeochemical function of river networks, such as CO_2 outgassing and nutrient spiraling[38–42].

Other relevant implications of our results stem from the identification of the major physical determinants of the mean network persistency. Surface flow is the byproduct of the excess water drained by the upstream contributing catchment, as proposed by[12,21]. Thus, in line with these previous studies, we hypothesize that the mean network persistency represents an important climatic signature of river basins. Accordingly, $\bar{P}$, which was poorly correlated with drainage basin areas ($R^2 < 0.01$), was found to be strongly linked to the underlying climatic water balance, here represented by the effective precipitation, $P_t - ET$ (i.e., total precipitation minus the potential evapotranspiration during the surveyed periods), as shown by Fig. 2c. Despite the high correlation between effective precipitation and persistency (overall $R^2 = 0.79$), some scattering appears in the observational data. This scatter is attributed to two factors: (1) relevant inter-catchment differences of geological or morphometric features, as suggested by[21,43]; and (2) an uneven distribution of the survey dates that might bias the relationship between the observed mean network persistency and the average climatic conditions during the study period for some catchments (light grey dots in Fig. 2c). Nevertheless, we found a clear climatic signature with drainage density statistics: lower mean network persistencies and enhanced relative active length variability were observed in the drier catchments (with $CV_D > 1.5$ for $P_t - ET < 40$mm/month, as in the Turbolo site). Conversely, in the wettest site (Coweeta, where $P_t - ET > 160$mm/month), the mean network persistency approached unity and network dynamics are smoothed, with $CV_D \to 0$. This result offers novel insight on the impact of climate on the active stream length variability[44], and nicely complements existing modeling and empirical approaches for the characterization of the spatial patterns of flow persistency across a landscape[21,31,45] . Therefore, we believe that the proposed framework can provide useful insight into the impact of climate on the temporal changes of the active drainage density.

Implications for large-scale studies

Several studies have investigated the impact of rainfall regimes on the geomorphic drainage density, D_g[46–49]. However, the influence of hydroclimatic drivers on the active fraction of the network is not fully understood. Notwithstanding the variability of D_g across the study catchments (attributed to their geological diversity), our results confirm that the extent of active channel length is linked to the amount of excess precipitation in the contributing catchment, as previously proposed in the literature[12,31]. This suggests the emergence of distinctive ecohydrological patterns within different climatic regions of the world. The largest temporal variations in the active stream length were found in the sites characterized by intermediate climates (i.e., $40 < P_t - ET < 100$ mm/month and $0.4 < \bar{P} < 0.6$), where the standard deviation of the active length and the geomorphic drainage density are concurrently higher (Fig. 3). Crucially, for intermediate values of $P_t - ET$ both the overall dynamic channel length and its internal heterogeneity are enhanced. In these settings, in fact, the observed local persistencies ranged from 0 to 1 (Supplementary Information) revealing the presence of multiple expansion/contraction cycles that operate with diverse frequencies, from individual storms to seasons. This behaviour generates a gradient of spatially heterogeneous habitats, from predominantly terrestrial to lentic, widening the spectrum of adaptation strategies and increasing biodiversity[22]. In the driest site (Turbolo), the relative variability of D is much higher than in all other settings (Fig. 2b), as almost the entire network is dynamic. However, the mean active length is typically reduced because of the predominance of dry reaches experiencing episodic activation. The lower persistencies induced by limited water availability entail shorter dynamical lengths of streams, regardless of the pronounced temporal changes of flow conditions experienced by dry rivers[50]. The ability of our analytical framework to quantitatively describe this wide spectrum of behaviours suggests the general applicability of the proposed approach within large-scale studies and makes it a sound basis for developing more specific numerical tools aimed at interpreting or predicting channel network dynamics.

Our analysis elucidates the major implications of the observed hierarchical behaviour of temporary streams on the spatial statistics of the node states and the temporal dynamics of the flowing length. In particular, temporal changes of the active drainage density are linked to the catchment water balance through the mean persistency of the whole network, whereas observed spatial patterns of flowing streams maximize the spatial correlation of

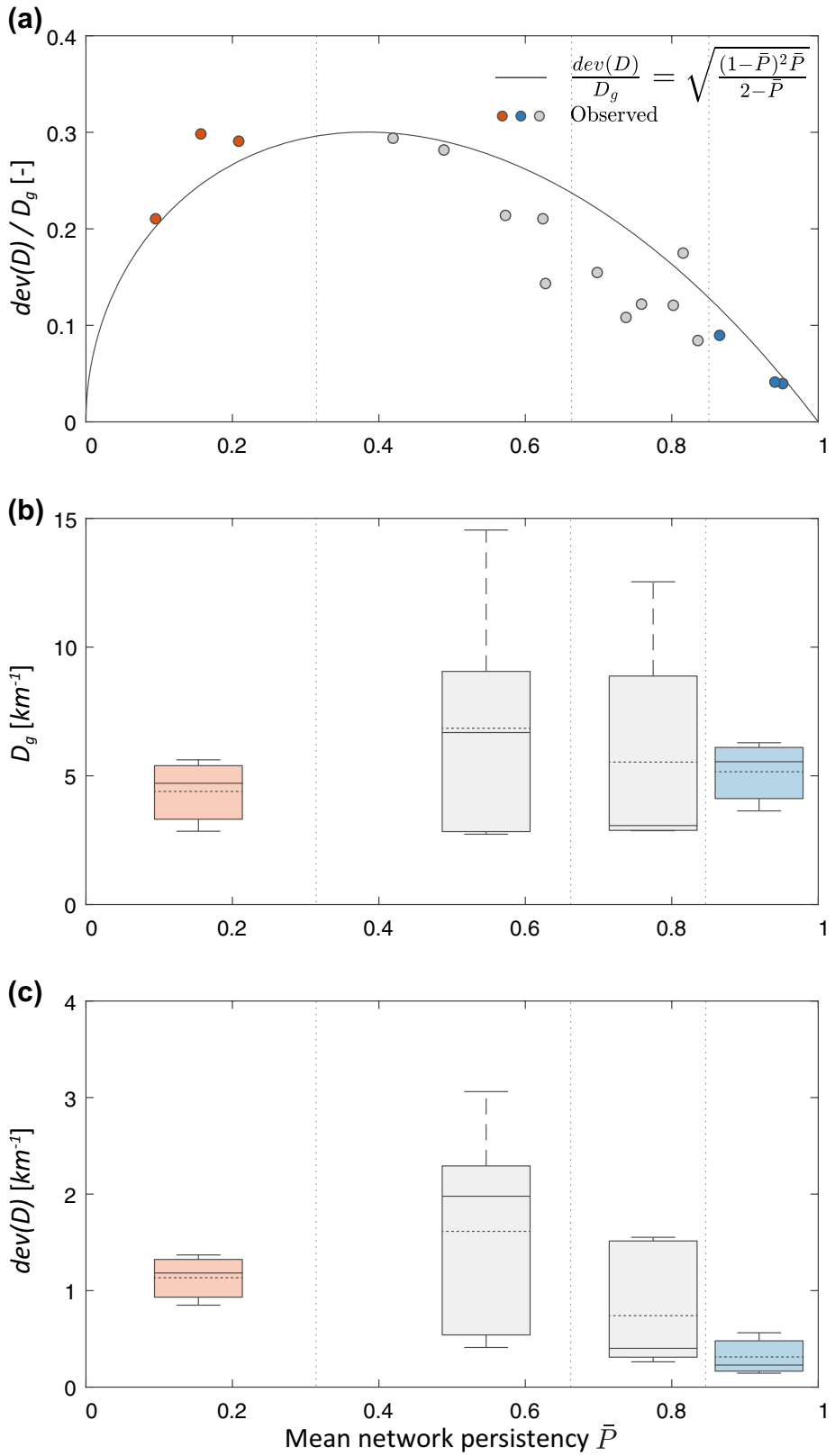

Figure 3. Dependence of key drainage density statistics on the mean network persistency, $\bar{P}$; the following statistics are shown in the three panels: (**a**) the standard deviation of the dynamic drainage density, $dev(D)$, scaled to the geomorphic drainage density, D_g; (**b**) the geomorphic drainage density; (**c**) the standard deviation of the active drainage density, that is proportional to the standard deviation of the active length through the contributing area. In panel (**a**) we show a comparison between observed values of $Dev(D)/D_g$ (dots) and the corresponding theoretical prediction of the analytical model as derived from Eqs. (1) and (4) for all the case studies where active lengths were monitored; in panels (**b**,**c**) the box-plots represent the first, second and third quartiles of observed data (solid lines) aggregated for different persistency ranges (as indicated by the dashed lines). The average is shown as a dotted line, while the full range is represented by whiskers.

the node states (wet vs. dry). The internal heterogeneity of the node persistency, though reflecting landscape complexity, is also modulated by climate and proves to be particularly enhanced under intermediate climatic conditions, leading to larger dynamical channel lengths in these settings. Furthermore, our study indicates that, because changes in wetness are generally synchronized, stream networks tend to be highly dynamic (i.e., they are nearly as dynamic as they can possibly be). Consequently, temporal variations of the active stream length and their climatic controls should be properly taken into account for accurate regional or global assessment of biogeochemical and ecological function of stream networks, particularly with changing climate.

Methods

Statistical moments of active length and drainage density

A river network is here represented as a sequence of N connected nodes, where the status of the node i ($i \in (1, N)$) identifies the hydrologic conditions within a stretch of stream length Δl_i. Without loss of generality, here the reach associated to the node i is not the link with one of the adjacent nodes but rather a stretch that embeds the node i. Accordingly, its length Δl_i is given by the sum of the semi-distances between the node i and all the connected neighbouring nodes. The status of each node corresponds to the status of the associated stretch and is represented by a binary random variable X_i, with $X_i = 1$ if the node experiences flowing water and $X_i = 0$ otherwise. Thus, the active network length can be expressed as: $L = \sum_{i=1}^{N} \Delta l_i \, X_i$. If, without loss of generality, we assume $\Delta l_i = \Delta \, l = const$ (i.e., equally spaced nodes), the mean active length can be calculated as:

$$\bar{L} = E[L] = N \ \Delta l \ E[X] = L_{max} \ \bar{P} \, , \tag{5}$$

where $E[-]$ denotes expectation, $\bar{P}$ is the mean network persistence and $L_{max} = N\Delta l$ is the geomorphic length (i.e. the maximum length of the network). Equation (5) and the Hortonian definition of drainage density, $D = L/A$ (A = catchment area) are then used to derive Eq. (1) in the main text (see Supplementary Information).

In this framework, the variance of the active length, $Var(L)$, is linked to the covariances $Cov(X_i, X_j)$ between the status of all the pairs of nodes as:

$$Var(L) = \Delta l^2 \sum_{i=1}^{N} \sum_{j=1}^{N} Cov(X_i, X_j) \, . \tag{6}$$

Under the assumption of hierarchical activation of the nodes[51], the covariance between X_i and X_j only depends on the persistency of the nodes i and j:

$$Cov(X_i, X_j) = Cov(X_j, X_i) = \begin{cases} P_j(1 - P_i) \ if \ P_i \geq P_j \\ P_i(1 - P_j) \ otherwise \end{cases} \tag{7}$$

Without loss of generality, we enumerate the nodes in a way such that $P_i \geq P_j$ whenever $i < j$. Combining Eqs. (6) and (7), $Var(L)$ can be thus expressed as (Supplementary Information):

$$\begin{aligned} Var(L) &= \Delta l^2 \left[\sum_{i=1}^{N} P_i(1 - P_i) + 2 \sum_{i=2}^{N} \sum_{j=1}^{i-1} P_j(1 - P_i) \right] \\ &\simeq L_{max}^2 \left[\bar{P}(1 - \bar{P}) + \widetilde{\Delta P} \right] , \end{aligned} \tag{8}$$

which leads to Eq. (2) in the main text. If the local persistency is uniform ($P_i = \bar{P}$), then $\widetilde{\Delta P} = 0$ in Eq. (8); under these circumstances, combining Eqs. (8) and (5) we obtain the upper theoretical limit for the coefficient of variation of the drainage density (and of the active length) expressed by Eq. (3). This limit also holds for non-hierarchical networks, since any departure from the hierarchical behavior would further decrease the observed CV_L and CV_D (see below).

Empirical data suggest that the local persistency along a network can be in most cases represented by a beta distribution with the first shape parameter equal to 1. Under this assumption, the term $\widetilde{\Delta P}$ in Eq. (8) reads (Supplementary Information):

$$\widetilde{\Delta P} = -\frac{\bar{P}(1 - \bar{P})}{2 - \bar{P}} \tag{9}$$

and combining Eqs. (9) and (2), CV_D takes the form shown in Eq. (4) of the main text.

The hierarchical activation scheme maximizes the spatial correlations and the temporal variability of L. In the general case, the covariance between X_i and X_j can be expressed as (Supplementary Information):

$$Cov(X_i, X_j) = P_j(1 - P_i) - P_{01} \, , \tag{10}$$

where P_i, P_j are, respectively, the marginal probabilities that the nodes i and j are active (i.e. the persistency of the nodes i and j) and $P_{01} = Prob[X_i = 0 \ and \ X_j = 1]$ is the joint probability that, at a given time, the node i is dry and the node j is active. As the covariance is symmetrical, without loss of generality let us assume $P_i \geq P_j$. For hierarchical networks, the less persistent node (j) can be active only if the more persistent node (i) is active. This implies $P_{01} = 0$ in Eq. (10), thereby leading to the maximization of $Cov(X_i, X_j) \, \forall \, (i, j)$. Thus, for a given set of

local persistencies, the hierarchical behaviour maximizes the covariance and the spatial correlation of the states of each pair of nodes. This implies that the mean spatial correlation within the entire network is maximized. Consequently, when the node activation in a temporary stream is hierarchical, the variance of the active length (and that of the drainage density) is maximized, as per Eq. (6).

Study catchments and empirical data. Our empirical dataset refers to 19 different catchments in Europe and USA, spanning a wide range of latitudes, climates, land covers, geologies and sizes (see Fig. 1 and Supplementary Information). This selection includes most of the monitoring sites where observational data on the temporal changes of the active network length are available for more than one season with an average resolution exceeding one survey per month. In the USA, 12 catchments (indicated with the capital letters *P*, *H*, *F* and *C* in Fig. 2 and in the main text) were selected that cover 4 different physiographic provinces of the Appalachian Highlands with different bedrock types and structure. The mean annual precipitation is between 1000 and 1800 mm, with catchment areas ranging between 12 and 70 ha. Maps of the flowing network were obtained from visual inspection during 7 surveys in 2015-2016[28]. In northern Italy, the Valfredda catchment (labelled as *V*) has been monitored 9 times during the summer and fall of 2018. This catchment has an area of 5.3 km^2 and highly variable geology consisting of morains, tallus slopes, and carbonate and siliciclastic bedrock. The climate is alpine, with a mean annual precipitation of approximately 1500 mm[27]. In spite of the wet climate, the stream network contains three reaches that are permanently disconnected to the outlet. This is the result of a strong physiographic heterogeneity of the contributing catchment, which determine a local increase of the soil storage capacity in the northern portion of the basin. Three additional catchments in southern Italy (labelled as *T*) were also considered, with drainage areas of 67, 48 and 24 ha. Therein, the active network has been monitored on average 38 times in 2019 and early 2020. Despite significant inter-catchment morphological heterogeneities, these sites are all characterized by sandy-conglomerate formations and a fractured crystalline-metamorphic bedrock. The climate of the region is Mediterranean, with a mean annual precipitation around 1300 mm and hot, dry summers. The largest study catchments of this paper are the Attert (247 km^2, Luxembourg) and the Seugne (920 km^2, western France), where available data quantify flow presence in a number of sparse nodes (182 for the Attert and 40 for the Seugne). The Attert catchment, consisting of slate, marls, and sandstones, was monitored using water presence sensors at sub-hourly temporal resolutions from 2013 to 2017. In this region, the climate is characterized by mild summers and wet winters[52] and the mean annual precipitation is 850 mm. The Seugne catchment was monitored monthly via visual inspections from 2012 to 2020. The main geologic units of this catchment include limestones, carbonates sedimentary rocks and sand, whereas the climate is Marine West Coast, with a mean annual precipitation around 850 mm evenly distributed throughout the year. The data of the Attert and the Seugne were used only for the validation of the hierarchical model because the active lengths were not monitored.

Calculation of relevant hydrologic and climatic indexes. For each case study where active stream maps were available, the network was represented by a large number of equally spaced nodes (on average 1250 nodes per km^2 of contributing area), that were assumed as representative of the hydrological status of a homogeneous reach in between two or more connected nodes. The nodes were designed to represent the full geometry of the geomorphic network, here defined as the maximum possible extension of the stream network. While there are small differences across the study sites in the procedure used to estimate the geomorphic network, in all cases the latter was obtained from field surveys and included the sites that were dry during the surveys but showed clear evidence of channelization. For each field survey, the active length was calculated as the sum of the individual lengths associated with all the active nodes in the network. Then, for each catchment, the sample mean and variance of L were used to estimate $\bar{L}$ and $var(L)$. The local persistency of node i, P_i was calculated as the fraction of times in which that node was observed as active during the surveys. Likewise, the mean network persistency $\bar{P}$ was then computed as the spatial average of the local persistency P_i. For each catchment, the time between any possible pair of mapping dates was also calculated, and the median time τ_m was estimated to assess the potential bias introduced by an uneven distribution of the dates when active lengths were mapped. The climatic water balance was analyzed for each case study, and the effective precipitation, $P - ET$, was calculated as the difference between precipitation and potential evapotranspiration (Supplementary Information).

Accuracy of the hierarchical model . The hierarchical model assumes that the activation of the nodes follows a descending persistency order. This implies that, at any given time, there exists a persistency threshold P^* that allows a separation between the dry nodes ($P < P^*$) and the wet nodes ($P \geq P^*$). Accordingly, hierarchical active networks were constructed assuming that, at any given time t, each node was active if and only if its local persistency was bigger than a suitable, time-dependent threshold $P^*(t)$. For each field survey, P^* was calculated as the exceedance probability of the corresponding observed number of active nodes. To compare observed and hierarchical active networks, a confusion matrix was computed for each node of each study catchment. The modeled and observed states of each node within all the field surveys were then compared. The spatially and temporally averaged accuracy of the hierarchical model was then calculated as

$$Accuracy = \frac{TP + TN}{TP + TN + FP + FN} \tag{11}$$

where TP, TN, FP and FN indicate, respectively, the true positives (i.e. the number of nodes and times for which the status of a node is correctly modeled as active), the true negatives, the false positives and the false negatives. An accuracy of 100% means that the hierarchical model was able to correctly model the status of all the nodes in

the network during all the field surveys. The local accuracy shown in the insets of Fig. 1b was defined analogously, the only difference being that it refers to a single node, instead of the whole network.

Data availability

The network monitoring data analyzed in this study is publicly available at[53]. All the data about the Attert catchment can be found in[54]. Data about the Seugne catchment is part of the ONDE dataset[55]. Additional information about the catchments can also be found in the Supplementary Information.

Received: 16 March 2021; Accepted: 20 October 2021
Published online: 02 November 2021

References

1. Battin, T. J. *et al.* Biophysical controls on organic carbon fluxes in fluvial networks. *Nat. Geosci.* **1**, 95–100. https://doi.org/10.1038/ngeo101 (2008).
2. Rinaldo, A., Gatto, M. & Rodriguez-Iturbe, I. River networks as ecological corridors: A coherent ecohydrological perspective. *Adv. Water Resour.* **112**, 27–58. https://doi.org/10.1016/j.advwatres.2017.10.005 (2018).
3. Montgomery, D. R. & Dietrich, W. E. Where do channels begin?. *Nature* **336**, 232–234. https://doi.org/10.1038/336232a0 (1988).
4. Montgomery, D. R. & Dietrich, W. E. Source areas, drainage density, and channel initiation. *Water Resour. Res.* **25**, 1907–1918. https://doi.org/10.1029/WR025i008p01907 (1989).
5. Kirchner, J. W. Statistical inevitability of Horton's laws and the apparent randomness of stream channel networks. *Geology* **21**, 591–594. https://doi.org/10.1130/0091-7613(1993)021<3c0591:SIOHSL>3e2.3.CO;2 (1993).
6. Rinaldo, A. *et al.* Self-organized fractal river networks. *Phys. Rev. Lett.* **70**, 822–825. https://doi.org/10.1103/PhysRevLett.70.822 (1993).
7. Banavar, J. R., Maritan, A. & Rinaldo, A. Size and form in efficient transportation networks. *Nature* **399**, 130–132. https://doi.org/10.1038/20144 (1999).
8. Sassolas-Serrayet, T., Cattin, R. & Ferry, M. The shape of watersheds. *Nat. Commun.* **9**, 3791. https://doi.org/10.1038/s41467-018-06210-4 (2018).
9. Yi, R. S. *et al.* Shapes of river networks. *Proc. R. Soc. A*https://doi.org/10.1098/rspa.2018.0081 *(2018).*
10. Rodriguez-Iturbe, I. & Rinaldo, A. *Fractal River Basins: Chance and Self-Organization* (Cambrige University Press, 1997).
11. Acuna, V. *et al.* Why should we care about temporary waterways?. *Science*https://doi.org/10.1126/science.1246666 *(2014).*
12. Godsey, S. E. & Kirchner, J. W. Dynamic, discontinuous stream networks: Hydrologically driven variations in active drainage density, flowing channels and stream order. *Hydrol. Process.* **28**, 5791–5803. https://doi.org/10.1002/hyp.10310 (2014).
13. Zimmer, M. A. *et al.* Zero or not? Causes and consequences of zero-flow stream gage readings. *WIREs Water*https://doi.org/10.1002/wat2.1436 *(2020).*
14. Datry, T., Bonada, N. & Boulton, A. J. Chapter 1: General Introduction. In *Intermittent Rivers and Ephemeral Streams* (eds Datry, T. *et al.*) 1–20 (Academic Press, 2017). https://doi.org/10.1016/B978-0-12-803835-2.00001-2.
15. Kiel, B. & BayaniCardenas, M. Lateral hyporheic exchange throughout the Mississippi River network. *Nat. Geosci.* **7**, 413–417. https://doi.org/10.1038/ngeo2157 (2014).
16. Mari, L. *et al.* Metapopulation persistence and species spread in river networks. *Ecol. Lett.* **17**, 426–434. https://doi.org/10.1111/ele.12242 (2014).
17. Burrows, R. M. *et al.* High rates of organic carbon processing in the hyporheic zone of intermittent streams. *Sci. Rep.*https://doi.org/10.1038/s41598-017-12957-5 *(2017).*
18. Datry, T. *et al.* Flow intermittence and ecosystem services in rivers of the Antropocene. *J. Appl. Ecol.* **55**, 353–364. https://doi.org/10.1111/1365-2664.12941 (2017).
19. Stubbington, R. *et al.* Temporary streams in temperate zones: Recognizing, monitoring and restoring transitional aquatic-terrestrial ecosystems. *Wiley Interdiscip. Rev. Water*https://doi.org/10.1002/wat2.1223 *(2017).*
20. Tonkin, J. D. *et al.* The role of dispersal in river network metacommunities: Patterns, processes, and pathways. *Freshw. Biol.* **63**, 141–163. https://doi.org/10.1111/fwb.13037 (2017).
21. Prancevic, J. P. & Kirchner, J. W. Topographic controls on the extension and retraction of owing streams. *Geophys. Res. Lett.* **46**, 2084–2092. https://doi.org/10.1029/2018GL081799 (2019).
22. Vander Vorste, R., Sarremejane, R. & Datry, T. Intermittent rivers and ephemeral streams: A unique biome with important contributions to biodiversity and ecosystem services. *Encyclopedia Worlds Biomes.* **1**, 419–429. https://doi.org/10.1016/B978-0-12-409548-9.12054-8 (2020).
23. Meyer, J. L. *et al.* The contribution of headwater streams to biodiversity in river networks. *J. Am. Water Resourc. Assoc.* **43**, 86–103. https://doi.org/10.1111/j.1752-1688.2007.00008.x (2007).
24. Leigh, C. *et al.* Ecological research and management of intermittent rivers: An historical review and future directions. *Freshw. Biol.* **61**, 1181–1199. https://doi.org/10.1111/fwb.12646 (2016).
25. Acuna, V., Hunter, M. & Ruhì, A. Managing temporary streams and rivers as unique rather than second-class ecosystems. *Biol. Conserv.* **221**, 12–19. https://doi.org/10.1016/j.biocon.2016.12.025 (2017).
26. Creed, I. F. *et al.* Enhancing protection of vulnerable waters. *Nat. Geosci.* **10**, 809–815. https://doi.org/10.1038/NGEO3041 (2017).
27. Durighetto, N. *et al.* Intraseasonal drainage network dynamics in a head water catchment in the Italian Alps. *Water Resour. Res.*https://doi.org/10.1029/2019WR025563 *(2020).*
28. Jensen, C. K., McGuire, K. J. & Prince, P. S. Headwater stream length dynamics across four physiographic provinces of the Appalachian Highlands. *Hydrol. Process.* **31**, 3350–3363. https://doi.org/10.1002/hyp.11259 (2017).
29. Fritz, K. M., Wenerick, W. R. & Kostich, M. S. A validation study of a rapid field-based rating system for discriminating among ow permanence classes of headwater steams in South Carolina. *Environ. Manag.* **52**, 1286–1298. https://doi.org/10.1007/s00267-013-0158-x (2013).
30. Prat, N. *et al.* The Mirage toolbox: An integrated assessment tool for temporary streams. *River Res. Appl.* **30**, 1318–1334. https://doi.org/10.1002/rra.2757 (2014).
31. Senatore, A. *et al.* Monitoring and modeling drainage network contraction and dry down in Mediterranean headwater catchments. *Water Resour. Res.*https://doi.org/10.1029/2020WR028741 *(2021).*
32. Lapides, D. A. *et al.* Variability of headwater stream network extents controlled by ow regime and network hydraulic scaling. *Hydrol. Process.*https://doi.org/10.1002/hyp.14079 *(2021).*
33. Horton, R. E. Erosional developement of streams and their drainage basins: Hydrophysical approach to quantitative morphology. *GSA Bull.* **56**, 275–370. https://doi.org/10.1130/0016-7606(1945)56[275:EDOSAT]2.0.CO;2 (1945).
34. Ilja van Meerveld, H. J. *et al.* Expansion and contraction of the owing stream network alter hillslope flowpath lengths and the shape of the travel time distribution. *Hydrol. Earth Syst. Sci.* **23**, 4825–4834. https://doi.org/10.5194/hess-23-4825-2019 (2019).

35. Fritz, K. M., Johnson, B. R. & Walters, D. M. Physical indicators of hydrologic permanence in forested headwater streams. *J. North Am. Benthol. Soc.* **27**, 690–704. https://doi.org/10.1899/07-117.1 (2008).
36. Gallart, F. *et al.* TREHS: An open-access software tool for investigating and evaluating temporary river regimes as a first step for their ecological status assessment. *Sci. Total Environ.* **607–608**, 519–540. https://doi.org/10.1016/j.scitotenv.2017.06.209 (2017).
37. Stubbington, R. *et al.* Biomonitoring of intermittent rivers and ephemeral streams in Europe: Current practice and priorities to enhance ecologi617 cal status assessments. *Sci. Total Environ.* **618**, 1096–1113. https://doi.org/10.1016/j.scitotenv.2017.09.137 (2018).
38. Raymond, P. A. *et al.* Global carbon dioxide emissions from inland waters. *Nature* **503**, 355–359. https://doi.org/10.1038/nature12760 (2013).
39. Gómez-Gener, L. *et al.* When water vanishes: Magnitude and regulation of carbon dioxide emissions from dry temporary streams. *Ecosystems* **19**, 710–723. https://doi.org/10.1007/s10021-016-9963-4 (2016).
40. Bertuzzo, E. *et al.* Scaling of dissolved organic carbon removal in river networks. *Adv. Water Resour.* **110**, 136–146. https://doi.org/10.1016/j.advwatres.2017.10.009 (2017).
41. von Schiller, D. *et al.* Sediment respiration pulses in intermittent rivers and ephemeral streams. *Glob. Biogeochem. Cycles* **33**, 1251–1263. https://doi.org/10.1029/2019GB006276 (2019).
42. Keller, P. S., Catalàn, N. & Marcé, R. Global CO2 emissions from dry inland waters share common drivers across ecosystems. *Nat. Commun.*https://doi.org/10.1038/s41467-020-15929-y *(2020).*
43. Stoll, S. & Weiler, M. Explicit simulations of stream networks to guide hydrological modelling in ungauged basins. *Hydrol. Earth Syst. Sci.* **14**, 1435–1448. https://doi.org/10.5194/hess-14-1435-2010 (2010).
44. Jaeger, K., Olden, J. & Pelland, N. Climate change poised to threaten hydrologic connectivity and endemic fishes in dryland streams. *Proc. Natl. Acad. Sci. USA* **111**, 13894–13899. https://doi.org/10.1073/pnas.1320890111 (2014).
45. Jensen, Carrie K. *et al.* Quantifying spatiotemporal variation in head water stream length using ow intermittency sensors. *Environ. Monit. Assess.* **4**, 191–226. https://doi.org/10.1007/s10661-019-7373-8 (2019).
46. Melton, M. A. An analysis of the relations among elements of climate, surface properties, an geomorphology. *Office Naval Res.* (1957).
47. Moglen, G. E., Eltahir, E. A. B. & Bras, R. L. On the sensitivity of drainage density to climate change. *Water Resour. Res.* **34**, 855–862. https://doi.org/10.1029/97WR02709 (1998).
48. Collins, D. B. G. & Bras, R. L. Climatic and ecological controls of equilibrium drainage density, relief, and channel concavity in dry lands. *Water Resour. Res.*https://doi.org/10.1029/2009WR008615 *(2010).*
49. Sangireddy, H. *et al.* Controls of climate, topography, vegetation and lithology on drainage density extracted from high resolution topography data. *J. Hydrol.* **537**, 271–282. https://doi.org/10.1016/j.jhydrol.2016.02.051 (2016).
50. Basso, S., Schirmer, M. & Botter, G. A physically based analytical model of flood frequency curves. *Geophys. Res. Lett.*https://doi.org/10.1002/2016GL069915 *(2016).*
51. Botter, G. & Durighetto, N. The stream length duration curve: A tool for characterizing the time variability of the owing stream length. *Water Resourc. Res.* **56**, 8. https://doi.org/10.1029/2020WR027282 (2020).
52. Kaplan, M. H. *et al.* Monitoring ephemeral, intermittent and perennial stream ow: A dataset from sites in the Attert catchment, Luxemburg. *Earth Syst. Sci. Data* **11**, 1363–1374. https://doi.org/10.5194/essd-11-1363-2019 (2019).
53. Botter G. et al. Taking the pulse of river networks: climate-driven dy- namics of the active channel length in temporary streams: DATASET. http://researchdata.cab.unipd.it/id/eprint/376. https://doi.org/10.25430/researchdata.cab.unipd.it.00000376.
54. Kaplan N. H. et al. Time series of stream ow occurrence from sites in ephemeral, intermittent and perennial streams in the Attert catchment, Luxembourg. https://dataservices.gfz-potsdam.de/caos/showshort.php?id=escidoc:4038898. https://doi.org/10.5880/FIDGEO.2019.010.
55. Observatoire national des étiages (ONDE) dataset. https://onde.eaufrance.fr.

Acknowledgements

We thank the Editor, Curt Storlazzi, and the two anonymous reviewers for their thorough commentary and valuable remarks that greatly improved the final version of the manuscript.

Author contributions

G.B. and N.D. conceived and designed research; G.B. and N.D. performed research; G.B., F.V., A.S., C.J., M.W., K.M., G.M. and N.D. analyzed and discussed results; N.D prepared Figures 1–3. G.B. wrote the paper with significant contributions from all authors.

Funding

Funding was provided by H2020 European Research Council (Grant No. 770999)

Competing interests

The authors declare no competing interests.

Additional information

Supplementary Information The online version contains supplementary material available at https://doi.org/10.1038/s41598-021-00922-2.

Correspondence and requests for materials should be addressed to G.B.

Reprints and permissions information is available at www.nature.com/reprints.

Publisher's note Springer Nature remains neutral with regard to jurisdictional claims in published maps and institutional affiliations.

Hierarchical climate-driven dynamics of the active channel length in temporary streams - Supplementary information

Gianluca Botter, Filippo Vingiani, Alfonso Senatore,
Carrie Jensen, Markus Weiler, Kevin McGuire,
Giuseppe Mendicino, Nicola Durighetto

June 2021

1 Supplementary Methods, Figures and Tables

1.1 Study catchments

The empirical dataset used in the paper comprises different experimental sites in Europe and USA. A summary description of each study site is reported below. Tables S1 reports key information about the field surveys performed in each study catchment. The long term climatic, hydrological and geo-lithological characteristics of the sites are reported in tables S2 and S3. Table S4 contains all the data relative to the study periods, as shown in Figures 2 and 3 of the main text..

Valfredda - The Valfredda catchment is located in the southern side of the Alps, in northern Italy. It has a contributing area of 5.3 km^2 and its altitudes range between 1500 and 3000 $ma.s.l.$, with steep slopes. The geomorphic network is 16.8 km long, corresponding to a geomorphic drainage density D_g of 3.16 km^{-1}. The geology and the physiography of the catchment are quite heterogeneous as reflected by the spatial variability of the local persistency throughout the network. Deposits of gravel and rocky debris dominate the upper part of the catchment, generating temporary channels with low persistency. In the lower part of the catchment, instead, the bedrock is covered by a vegetated soil layer. therein, the drainage density is higher and the streams are more persistent and dynamic. Conversely, in the central-eastern part of the catchment, the dolomite bedrock is exposed, generating dynamical streams with high slopes and a low persistency. The catchment experiences a typical alpine climate, with a mean annual precipitation of approximately 1500 mm. The summers are short and wet, with high rainfall frequencies, while the winters are long, cold and dominated by snow input. The active portion of the river network has been surveyed 14 times from July 2018 to May 2019; from Dec 2018 to may 2019, the network remained almost steady due to the winter freezing. The analysis of the available

data has been performed during the whole survey period (V_1) and then focussing only on the summer and fall seasons, that represent the period during which the network is more dynamic (July-Nov 2018, V_2). For more detailed information about the Valfredda catchment the reader is referred to [28].

Turbolo - The Turbolo creek is a small river located in southern Italy, where the climate is Mediterranean with hot summers; its drainage area is approximately 7 km^2 at the outlet of Fitterizzi, with elevations ranging between 183 and 1005 *ma.s.l.*. The empirical data used in this study refers to two subbasins in the northern part of the catchment, with contributing areas of 0.67 and 0.48 km^2 (catchments T_1 and T_3, respectively). A third catchment (T_2), nested into T_1, has also been identified to capture the effects of the internal heterogeneity of geology and land cover in the study area. The T_2 catchment drains an area of 0.23 km^2 only. The Mediterranean climate of the area consists in hot and dry summers with wet, mild winters. The annual precipitation is approximately 1200 mm, but due to high evapotranspiration rates a complete dry-down of the network is observed during the summer. The T catchments are dominated by silty marly clays with low permeability, that generate (jointly with the aridity of climate) streams with very low persistency. The geomorphic drainage densities in this site range between 2.8 and 5.6 km^2. The upper part of T_1 is composed by sandy-conglomerate formations, in which the higher permeability produce a relative increase in the persistency of the stream network. The catchments T_1 and T_2 have been monitored for 35 times from April 2019 to January 2020, while T_3 was monitored for 42 times from May 2019 to January 2020.

Hubbard Brook - Three US catchments considered in this study pertain to the Hubbard Brook Experimental Forest of New Hampshire (New England). In the paper, they have been identified as H_1, H_2 and H_3, and their contributing areas are 0.14, 0.25 and 0.42 km^2, respectively. The mean altitude of these catchments ranges between 630 and 740 *ma.s.l.*, with average slopes of 28%. The stream networks of these catchments are the densest of our dataset, with geomorphic drainage densities of 12.5, 14.5 and 8.9 km^{-1}, respectively. The geology of the sites is mainly composed of shists and granulites, covered by a mantle of sandy loams. The humid continental climate of the area provides a mean annual precipitation of 1400 mm, with cold snowy winters and mild summers. For each catchment, 7 visual monitoring of the active network have been carried out in June and July 2015, spanning a wide range of hydroclimatic conditions. More information on this catchments is available in [27].

Fernow - The Fernow Experimental Forest is located in the Appalachian Plateau of West Virginia (USA). In this site, three study catchments (F_1, F_2, F_3) have been selected, with drainage areas of 0.14, 0.16 and 0.37 km^2, respectively. These catchments have a mean altitude of approximately 800 *ma.s.l.*, with slopes around 30%. Field observations revealed geomorphic drainage densities of 2.9 km^{-1} with local persistencies varying in the full range between 0 and 1. The bedrock is composed of shales and sandstones, with a soil cover consisting mainly of silt loams. The average annual precipitation is approximately 1450 mm, with rainy summers and mite winters. Snowfalls are common but usually

limited and isolated. From May to December 2016 a total of 7 field surveys per catchment were carried out. More information on this study site can be found in [27].

Potts and Poverty - Three study catchments are located in the Valley and Ridge physiographic provinces of Virginia (USA). Two of them (P_1 and P_2) are part of the Poverty Creek, while the third (P_3) belongs to the South Fork Potts Creek, 25 km northern of P_1 and P_2. These catchments have a contributing area of 0.25, 0.35 and 0.73 km^2, respectively. P_1 and P_2 have and average elevation of 750 $ma.s.l.$, a mean slope of 33% and a geomorphic drainage density of 7 km^{-1}. The Potts Creek catchment, instead, has a higher elevation (1030 $ma.s.l.$) and gentler slopes (27%). Its geomorphic drainage density is 2.9 km^{-1}. Bedrocks are mainly composed by standstones in all the catchments, whereas shales and siltstones can be found in the P_1 and P_2 sites. The average annual precipitation in the area is close to 1000 mm, remarkably lower than all the other USA catchments considered in this study (and comparable with the T sites in southern Italy). Unlike the Turbolo Creek, however, the drainage networks do not experience summer dry down due to the lower evapotranspiration rates. The active network in these catchment has been monitored by visual inspection 7 times between September 2015 and March 2016. More information about these study sites can be found in [27].

Coweeta - The C_1, C_2 and C_3 catchments are located in the Coweeta Hydrologic Laboratory, North Carolina (USA). They are the highest and steepest USA sites considered in this study, with mean elevations between 800 and 1100 $ma.s.l.$ and slopes of about 50%. These sites have areas of 0.12, 0.33 and 0.40 km^2, respectively, and drainage densities ranging between 3.6 and 6.2 km^{-1}. The catchments lie on the Southern Blue Ridge Mountains, which mainly consist of exposed metamorphic rock (biotite gneiss and amphibolite). The climate is generally warm and humid, with temperatures above $0°C$ all year round. The precipitation is greatest in winter and early spring, with an average annual precipitation of about 1800 mm. The field campaign for detecting the active stream network in these sites were carried out from November 2015 to December 2016, and consisted in 7 field surveys for each catchment. More information about these study sites can be found in [27].

Attert - The Attert catchment (cathcment code A) covers an area of 247 km^2 between Luxemburg and Belgium. The altitude ranges between 245 and 550 $ma.s.l.$ and the geology is dominated by slate, marls and sandstone, while lithology is driven by land use (mainly forest and agricolture). The climate is characterized by wet winters and mild summers, with an average annual precipitation of 900 mm uniformly distributed troughout the year (*58*). Different types of sensors were employed in this catchment (time-lapse photography, conductivity sensors and water level gauging stations) to monitor flow presence in a set of 182 nodes along the network. These sensors recorded water presence at a 30-minute time interval from 2013 to 2017. The sparse arrangement of the sensors along the network didn't allow a proper calculation of the active length. Therefore this data was only used to validate the hypothesis of hierarchical activation of the stretches. Detailed information about this catchment can be found

in [56].

Seugne - The Seugne river is located in the Charente-Maritime département in west France. The catchment (hereafter coded as S) has a contributing area of 920 km^2, with elevations that span between 8 and 160 $ma.s.l.$. The geology is composed of limestones, carbonates, sedimentary rocks and sand. The climate is Marine West Coast. The active network was monitored in the catchment as part of the Onde campaign. Visual inspection observations were employed determine water presence in a set of 40 predetermined nodes, at a monthly interval from 2012 to 2020. As for the Attert catchment, this data was only used for validating the hierarchical hypothesis because the sparse monitoring points did not allow the calculation of the active length. More information about the field campaign can be found in (*59*).

Table S1: Characteristics of the field campaigns carried out for the monitoring of the active stream network and accuracy of the hierarchical model.

Catchment code	Area $[km^2]$	**Survey type**	**# of surveys**	**Survey period**		**# of noeds**	τ_m $[days]$	**Accuracy**	Reference (watershed number[a])
A	247	ER sensors	33770	Aug-2015	Jul-2017	182	—	94%	Kaplan et al. 2019
C_1	0.12	Visual	7	Nov-2015	Dec-2016	323	146	100%	Jensen et al. 2017 (WS 18)
C_2	0.33	Visual	7	Nov-2015	Dec-2015	365	133	100%	Jensen et al. 2017 (WS 34)
C_3	0.4	Visual	7	Dec-2015	Dec-2016	707	128	100%	Jensen et al. 2017 (WS 32)
F_1	0.14	Visual	7	Jun-2016	Dec-2016	175	13	100%	Jensen et al. 2017 (WS 13)
F_2	0.16	Visual	7	May-2016	Dec-2016	243	14	100%	Jensen et al. 2017 (WS 10)
F_3	0.37	Visual	7	May-2016	Dec-2016	489	14	100%	Jensen et al. 2017 (WS 4)
H_1	0.14	Visual	7	Jun-2015	Jul-2015	861	13	100%	Jensen et al. 2017 (WS 6)
H_2	0.2	Visual	7	Jun-2015	Jul-2015	1429	10	100%	Jensen et al. 2017
H_3	0.43	Visual	7	Jun-2015	Jul-2015	2218	14	100%	Jensen et al. 2017 (WS 3)
P_1	0.25	Visual	7	Sep-2015	Jan-2016	1045	41	100%	Jensen et al. 2017
P_2	0.35	Visual	7	Sep-2015	Dec-2015	1225	23	100%	Jensen et al. 2017
P_3	0.73	Visual	7	Aug-2015	Mar-2016	906	61	100%	Jensen et al. 2017
S	920	Visual	78	Apr-2012	Oct-2019	40	—	96%	ONDE Dataset
T_1	0.63	Visual	35	Apr-2019	Jan-2020	368	75	99%	This study
T_2	0.23	Visual	35	Apr-2019	Jan-2020	173	75	99%	This study
T_3	0.46	Visual	42	May-2019	Jan-2020	205	67	99%	This study
V_1	5.27	Visual	14	Jul-2018	May-2019	504	82	97%	This study
V_2	5.27	Visual	9	Jul-2018	Nov-2018	504	40	96%	Durighetto et al. 2020

[a] If applicable, for gauged catchments at the experimental forests with a designated watershed number

Table S2: Summary of the main climatic and hydrological characteristics of the study catchments (NA = data not available). Note that the mean climatic attributes reported here are long term averages and do not refer to the study period only.

Catchment code	**Area** $[ha]$	**Mean elevation** $[ma.s.l.]$	**Mean temperature** $[^{\circ}C]$	**Mean precipitation** $[mm/month]$	**Mean evapotranspiration** $[mm/month]$	**Mean streamflow** $[mm/month]$	**Runoff coefficient**	**Aridity index**
A	24700	350	9.6	74.6	51.3	36.3	0.47	1.45
C_1	12	823	13.7	226.0	68.2	172.5	0.76	3.31
C_2	33	1019	13.8	229.7	77.8	160.5	0.70	2.95
C_3	40	1052	11.9	285.3	56.1	214.4	0.75	5.08
F_1	14	773	15.6	144.1	83.0	58.1	0.40	1.74
F_2	16	767	15.6	144.9	86.4	40.4	0.28	1.68
F_3	37	822	15.6	146.5	86.4	39.5	0.27	1.69
H_1	14	690	16.2	163.7	104.2	87.2	0.53	1.57
H_2	20	740	17.1	209.8	119.0	117.1	0.56	1.76
H_3	43	632	16.2	162.8	103.4	85.2	0.52	1.57
P_1	25	750	10.1	73.2	55.8	69.4	0.95	1.31
P_2	35	729	14.2	77.4	69.0	32.1	0.41	1.12
P_3	73	1029	NA	NA	36.4	57.6	NA	NA
S	91950	100	17.3	62.7	NA	NA	NA	NA
T_1	63	263	17.2	87.8	109.5	47.6	0.54	0.80
T_2	23	250	17.2	87.8	109.5	47.6	0.54	0.80
T_3	46	358	17.6	88.3	112.9	48.9	0.55	0.78
V_1	527	2250	7.6	152.7	47.8	86.4	0.57	3.19
V_2	527	2250	13.8	197.8	64.6	119.0	0.60	3.06

Table S3: Summary of the geology and soil use of the study catchments.

Catchment code	**Mean elevation** [*ma.s.l.*]	**Geology**	**Soil use**
A	350	Marl, slate and sandstone	Annual crops, fruit trees and mixed forests
C_1	823	Gneiss	Deciduous forest
C_2	1019	Gneiss	Deciduous forest
C_3	1052	Gneiss	Deciduous forest
F_1	773	Shale rocks	Deciduous forest
F_2	767	Shale rocks	Deciduous forest
F_3	822	Shale rocks	Deciduous forest
H_1	690	Mudstone and shists	Deciduous forest
H_2	740	Mudstone and granite	Evergreen and mixed forest
H_3	632	Shists and mudstone	Evergreen and deciduous forest
P_1	750	Shale rocks	Deciduous forest
P_2	729	Shale rocks	Deciduous forest
P_3	1029	Sandstones	Deciduous forest
S	100	Limestones	Annual crops, fruit trees and deciduous forests
T_1	263	Clays	Annual crops and fruit trees
T_2	250	Clays	Annual crops and fruit trees
T_3	358	Clays	Annual crops and steady meadows
V_1	2250	Limestone and sandstone	Natural pastures, coniferous forest and rocks
V_2	2250	Limestone and sandstone	Natural pastures, coniferous forest and rocks

1.2 Local persistency of the study catchments

Figure S1 shows the frequency distribution of the local persistency of the nodes within each study catchment (histograms). The plots also show as a solid line the fitted Beta distribution (see equation (S11)). Furthermore, the corresponding spatial maps of local persistency are represented in Figure S2.

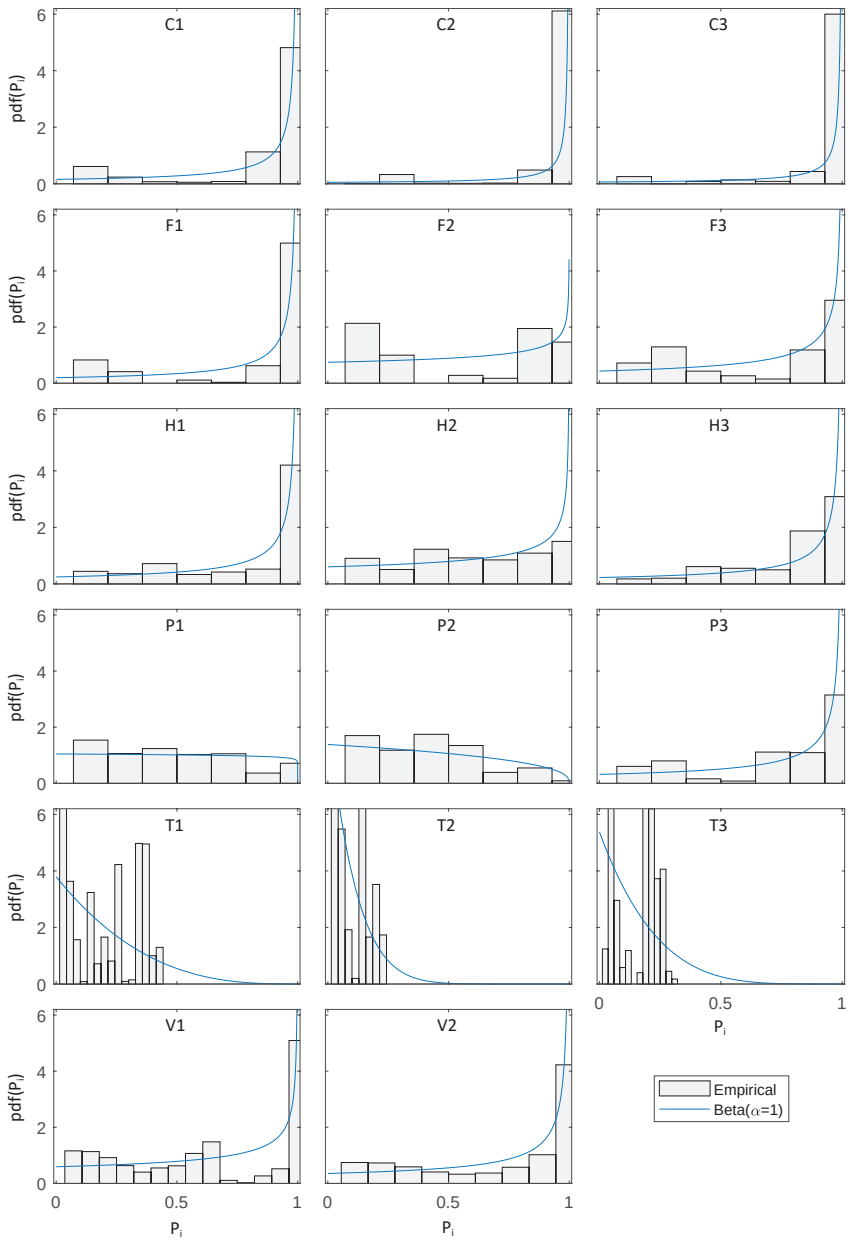

Figure S1: Probability Density Function of the local persistency P_i of the study catchments.

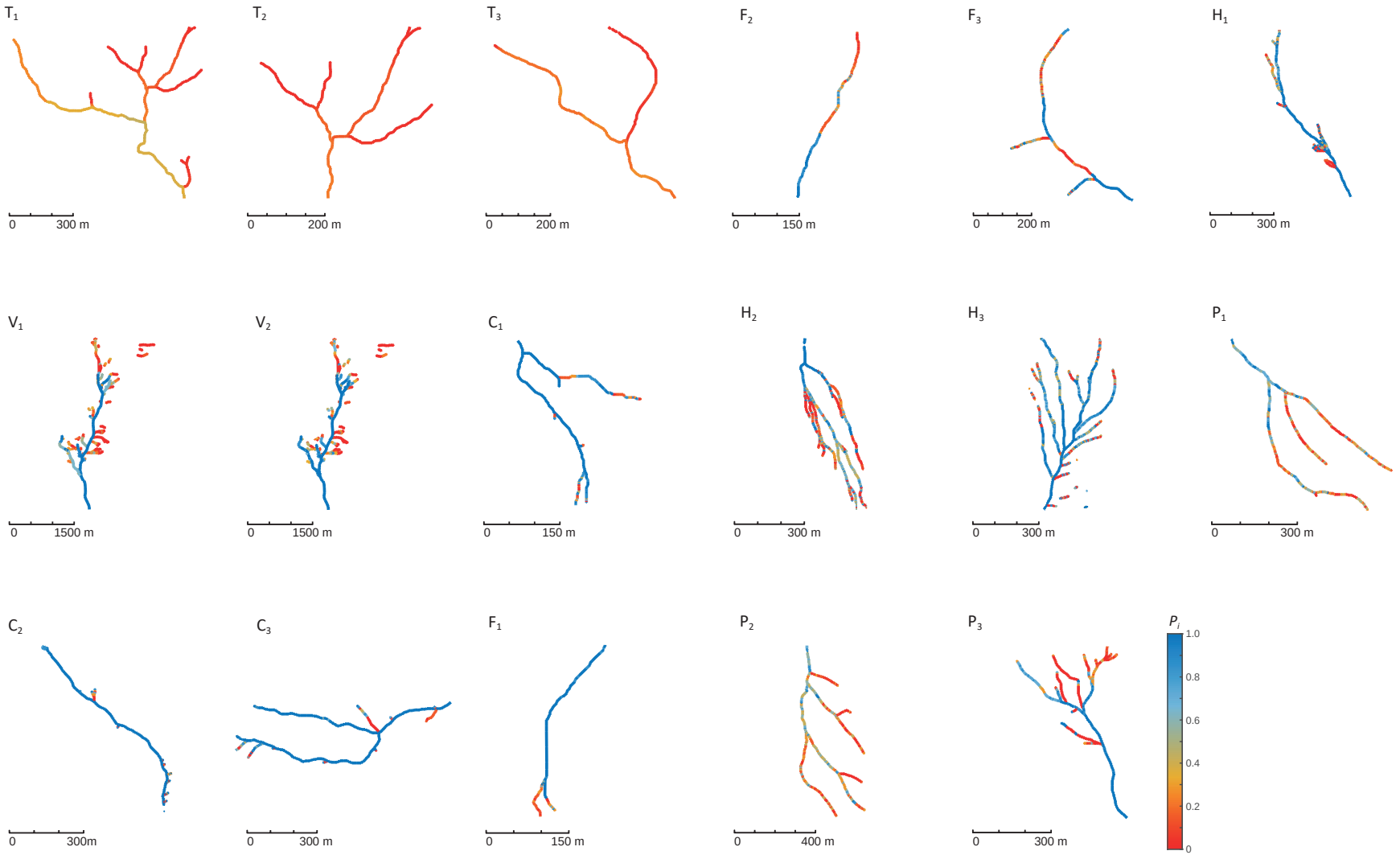

Figure S2: Maps of local persistency of the study catchments.

1.3 Climatic and morphologic features of the study catchments

Figure S3 summarizes the main climatic and hydrological characteristics of the study catchments reported in Table S2. The figures indicate that the study catchments cover a wide range of climatic conditions in terms of mean precipitation, evapotranspiration, aridity, temperature, catchment area and elevation. Therefore, the dataset can be considered as representative of a broad range of climatic and morphologic settings.

1.4 Methods underlying Figure 2c in the main text

Calculation of $P_t - ET$

The effective precipitation $P_t - ET$ is used in this paper to quantify the specific (per unit catchment area) catchment water availability. $P_t - ET$ is calculated as the difference between the total precipitation and the potential evapotranspiration temporally averaged over a suitable reference period. Specifically, the reference period consists of the months during which the field surveys for the network monitoring have been carried out. If a field survey was performed in the first 8 days of the month, the month before the first survey of the campaign has been included in the computation of $P_t - ET$. For the Italian catchments, climatic data necessary for the calculation of $P_t - ET$ were retrieved from the nearest Regional Environmental Protection Agency weather station (the Falcade station of ARPAV for the V catchment and the Fitterizzi station of ARPACAL fot the T catchment). Precipitation and streamflow data in the H, F and C catchments, instead, were provided by the Hubbard Brook Experimental Forest (*60*), the Fernow Experimental Forest (*61*) and the Coweeta Hydrologic Laboratory (*62*) respectively. Data from the NOAA meterologic station US1VAMN0025 were also used for the P_1 and P_2 catchments. No precipitation data were available for P_3 instead. Monthly potential evapotranspiration data for all the US catchments were provided by USGS (*63*). This data were estimated at a 1 km spatial scale using the SSEBop model, starting from climatic and morphological data (*64*). Instead, the Penman-Monteith equation was used to estimate the potential evapotranspiration in the T and V catchments, based on available climatic data (*65*).

Calculation of τ_m

The interarrival between any pair of field surveys is here defined as the time elapsed between the dates of the corresponding surveys. For each study catchment, the interarrival between each couple of survey dates has been calculated (including all the couples of non-consecutive surveys). Then, the median interarrival, τ_m, has been computed to quantify to what extent a field campaign was biased by the presence of several surveys concentrated in a relatively short sub-period of the whole survey period (shown in Table S1). The median interarrival was chosen instead of the average interarrival to reduce the effect of field survey that were carried out many months later than all the other surveys. It was found that if τ_m is too small, the surveys reflect the hydrological conditions

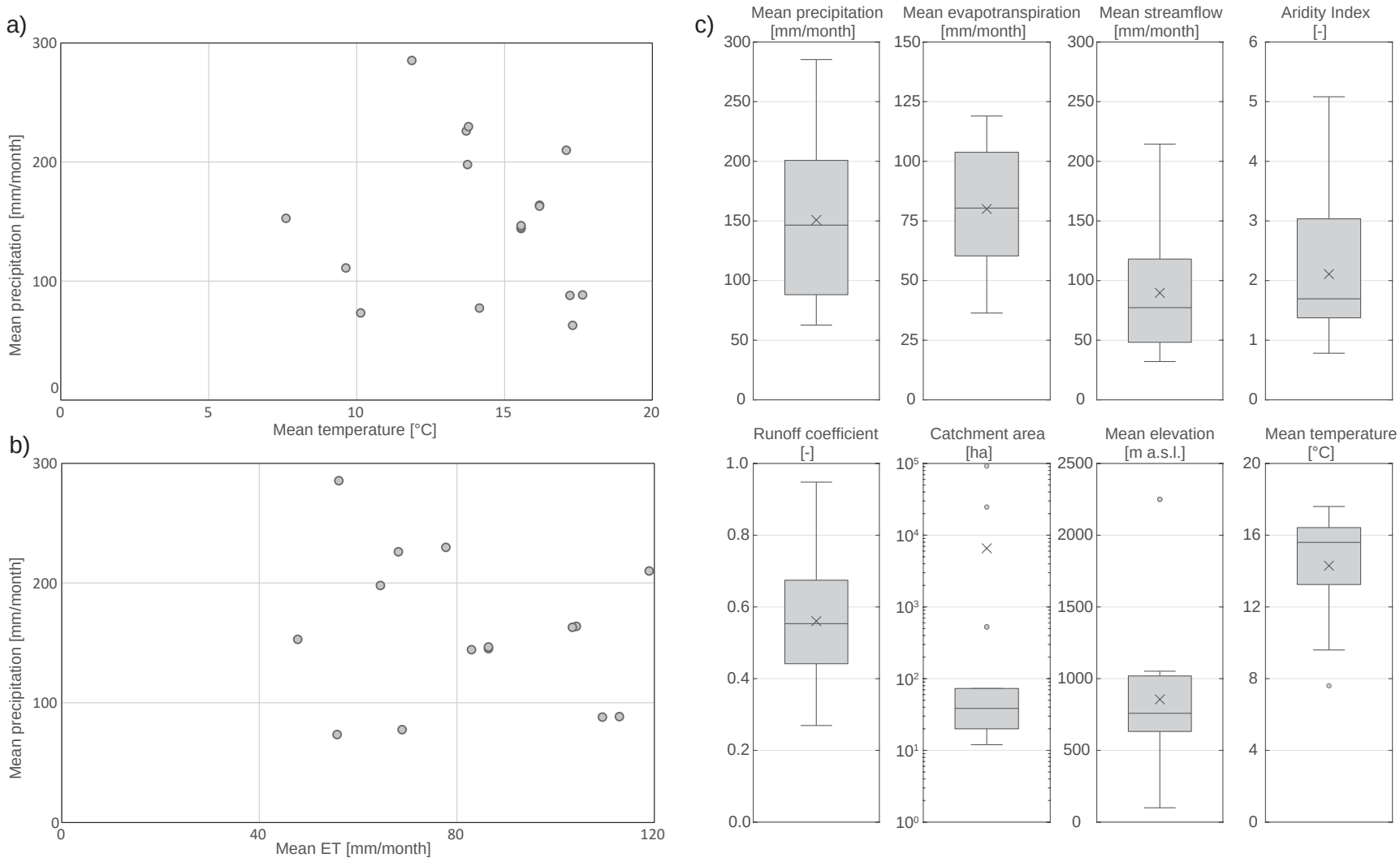

Figure S3: Representation of the study catchments in the Whittaker plot (mean annual temperature vs mean annual precipitation, panel a). Also shown is the scatter plot of the mean evapotranspiration and the mean annual precipitation across all the study sites (panel b). Panel c) shows box plots of the main climatic and morphologic characteristics of the study catchments.

observed during the months in which most of the surveys were performed and not the average climatic conditions over the whole study period. Considering that the mean frequency of the surveys is of the order of one survey per month, in this study it was assumed that τ_m must be greater than > 15 *days* to guarantee that the active lengths observed in correspondence of the field surveys can be properly linked to the average climatic conditions observed within all the months during which at least one survey was performed. The calculated values of τ_m for all the study catchments are reported in Table S1.

1.5 Performance of the hierarchical model

The accuracy of the hierarchical model on each of the study networks is calculated by means of equation (11) of the methods. Figure S5 shows the maps of the local accuracy of the hierarchical model for each study catchment. The Figures indicate that the local accuracy is close to 100% in most cases. The average accuracy within each study catchment is reported in Table 1. In the framework presented in this paper, the local persistency is calculated from empirical observations. Given that node persistency dictates the fraction of time for which a node is active, one could expect that a model in which each node is randomly activated/deactivated through time in a way that is consistent with the local persistency could have a positive accuracy. In fact, the accuracy of such a random model for a node with persistency P_i is $P_i^2 + (1 - P_i)^2$, leading to a minimum accuracy of 50%. The accuracy of the hierarchical model was thus compared to the accuracy of the random model for all the study catchments. Figure S6 show the maps of local accuracy that would be obtained from the random model. Figure S4 shows that the mean accuracy of the hierarchical model ($99 \pm 1.7\%$) is substantially higher than the accurcay of the random model ($79 \pm 7.5\%$).

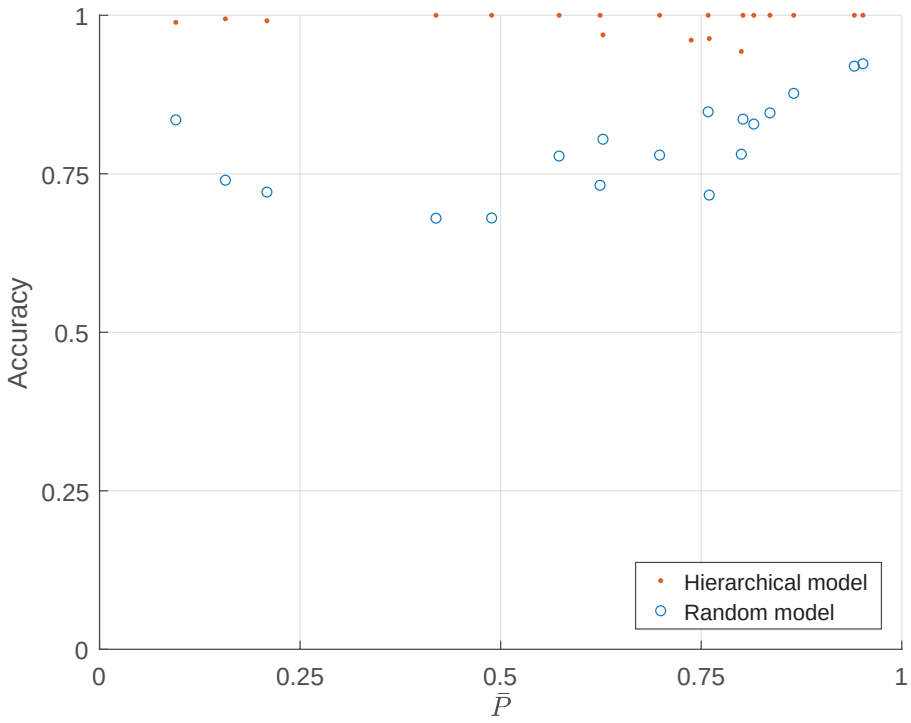

Figure S4: Accuracy of the hierarchical and random models as a function of the mean network persistency.

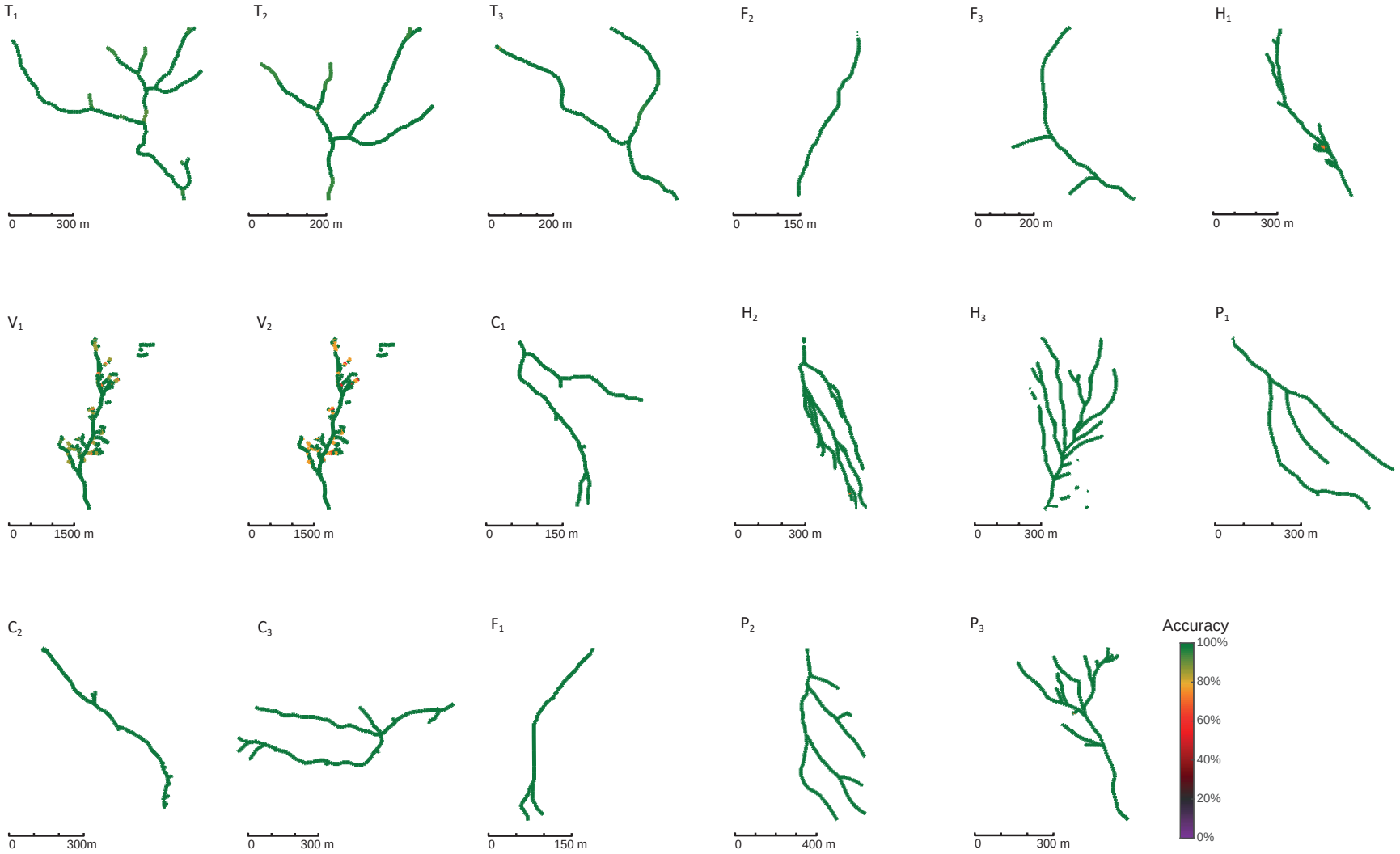

Figure S5: Maps of local accuracy of the hierarchical model for a set of the study catchments.

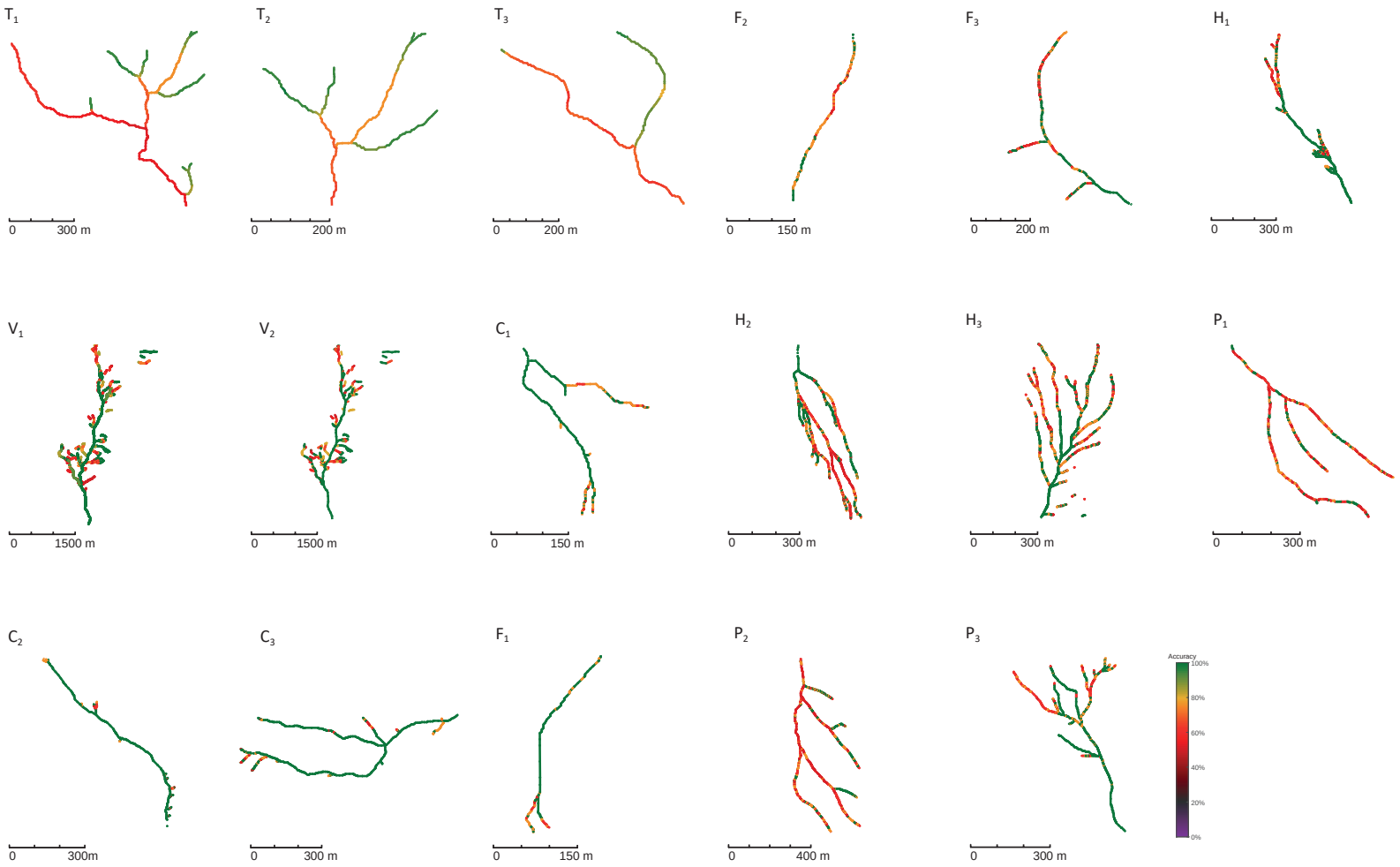

Figure S6: Maps of local accuracy of the random model.

1.6 Drainage density statistics

The data underlying Figures 2 and 3 of the main text are reported in Table S4, which reports the relevant drainage density statistics for the study catchments. The table also provides information on how the catchments have been grouped in the box and whiskers plots of Figure S3.

Table S4: Grouping of the study catchments and drainage density statistics

Group	Catchment code	$\bar{P}$	Area $[km^2]$	D_g $[km^{-1}]$	$\bar{D}$ $[km^{-1}]$	$dev(D)$ $[km^{-1}]$	$\bar{D}/D_g$	$dev(D)/D_g$	Mean precipitation $[mm/month]$	Mean ET $[mm/month]$
1	T2	0.10	0.23	5.62	0.52	1.18	0.09	0.21	99.4	114.2
	T3	0.16	0.46	2.85	0.45	0.85	0.16	0.30	99.4	114.2
	T1	0.21	0.63	4.71	0.97	1.37	0.21	0.29	99.4	114.2
2	P2	0.42	0.35	6.73	2.23	1.98	0.33	0.29	113.3	41.9
	P1	0.49	0.25	7.22	2.99	2.04	0.41	0.28	102.2	37.3
	F2	0.57	0.16	2.73	1.40	0.58	0.51	0.21	154.7	83.3
	H2	0.62	0.20	14.55	6.74	3.06	0.46	0.21	205.9	119.0
	V1	0.63	5.27	2.87	1.36	0.41	0.47	0.14	149.0	22.4
3	F3	0.70	0.37	2.92	1.62	0.45	0.55	0.15	155.1	83.3
	V2	0.74	5.27	2.87	1.59	0.31	0.56	0.11	172.4	25.9
	P3	0.76	0.73	2.88	1.46	0.35	0.51	0.12	NA	NA
	H1	0.80	0.14	12.54	8.62	1.51	0.69	0.12	198.5	73.0
	H3	0.82	0.43	8.88	6.46	1.55	0.73	0.17	197.9	118.8
	F1	0.84	0.14	3.11	2.49	0.26	0.80	0.08	140.1	71.7
4	C1	0.87	0.12	6.29	5.22	0.56	0.83	0.09	242.4	83.8
	C3	0.94	0.40	5.55	4.78	0.23	0.86	0.04	240.0	69.1
	C2	0.95	0.33	3.64	3.24	0.14	0.89	0.04	246.3	62.2

1.7 Correlation between mean network persistency and catchment area

Our analyses indicated that mean network persistency and catchment area are poorly correlated, with a correlation coefficient of 0.06. The scatter plot of $\bar{P}$ vs. A is shown in Figure S7.

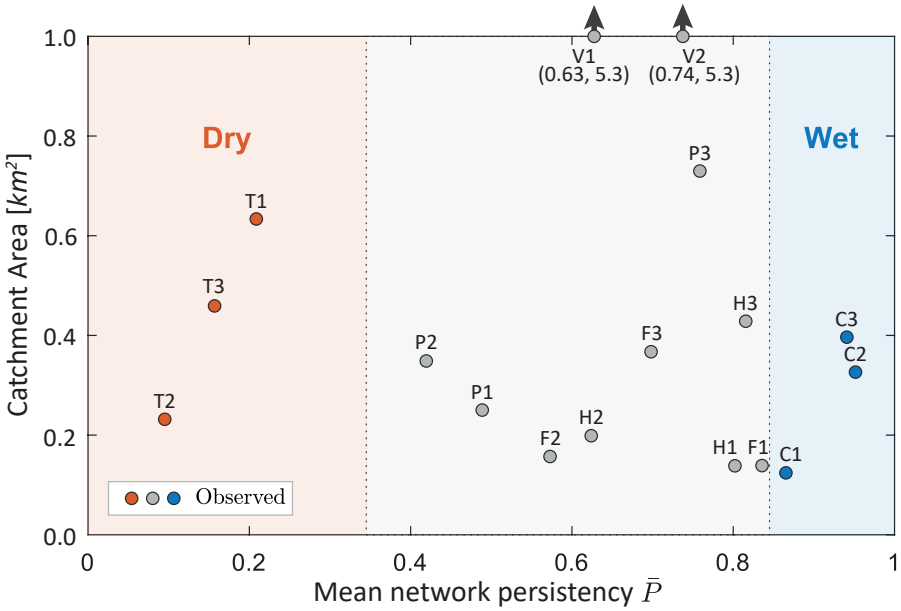

Figure S7: Scatter plot of catchment area and mean network persistency $\bar{P}$. The correlation coefficient is 0.06.

1.8 Analytical derivations

Average drainage density

A dynamical stream network is here described by a set of N nodes. Each node identifies the hydrological status (active vs. dry) of a suitably identified portion of stream network with length Δl_i. At any given time, the node i takes a binary status X_i (0 = dry / 1 = active). Therefore, at any time the active steam length can be calculated as the sum of the lengths associated to each active node,

$$L = \sum_{i=1}^{N} X_i \Delta l_i \ . \tag{S1}$$

The local persistency of node i, P_i, defined as the probability for the node i to be observed as active, can be calculated as the temporal average of the observed state of the node exploiting a series of field surveys of the active network (i.e. the average of X_i, sampled at different times).

Likewise, the average stream length can also be calculated as:

$$\bar{L} = \overline{\sum_{i=1}^{N} X_i \Delta l_i} = \sum_{i=1}^{N} \overline{X_i} \Delta l_i = \sum_{i=1}^{N} P_i \Delta l_i = \bar{P} L_g \tag{S2}$$

where $\bar{P}$ is the mean network persistency, $L_g = \sum_{i=1}^{N} \Delta l_i$ is the geomorphic length (corresponding to the length of the network when all the nodes are active), and the overline denotes time averaging. Equation (S2) shows that the definition of the maximum length of the network is a crucial step for the calculation of the mean persistency: in fact, for a given mean network length, the mean persistency is inversely proportional to L_{max}. Equation (1) of the main text is obtained by dividing both sides of equation (S2) by the catchment area.

General expression for the coefficient of variation of the active drainage density

The local status of each node, X_i, can be seen as a Bernoulli binary random variable. Accordingly, the local persistency is the expected value of X_i, while the variance of X_i can be expressed as: $Var(X_i) = P_i(1 - P_i)$. Let us now consider a generic couple of nodes i and j with local persistencies P_i and P_j, respectively. One can identify four joint probabilities of the states of these nodes as follows (*66*):

- $P_{11}^{ij} = Prob[X_i = 1 \; and \; X_j = 1]$
- $P_{00}^{ij} = Prob[X_i = 0 \; and \; X_j = 0] = 1 - P_j - P_i + P_{11}^{ij}$
- $P_{10}^{ij} = Prob[X_i = 1 \; and \; X_j = 0] = P_i - P_{11}^{ij}$
- $P_{01}^{ij} = Prob[X_i = 0 \; and \; X_j = 1] = P_j - P_{11}^{ij}$ (S3)

The above joint probabilities obey to three constraints: $P_{11}^{ij} + P_{10}^{ij} = P_i$, $P_{01}^{ij} + P_{11}^{ij} = P_j$ and $P_{11}^{ij} + P_{10}^{ij} + P_{01}^{ij} + P_{00}^{ij} = 1$. Incorporating these constraints into equation (S3) allows for the calculation of all the joint probabilities based on the local persistencies (P_i and P_j) and one joint probability (e.g. P_{11}^{ij}). In the general case, the covariance of the states of two nodes can be written as:

$$\begin{aligned} Cov(X_i, X_j) &= (1 - P_i)(1 - P_j)P_{11}^{ij} + (1 - P_i)(0 - P_j)P_{10}^{ij} + \\ &\quad (0 - P_i)(1 - P_j)P_{01}^{ij} + (0 - P_i)(0 - P_j)P_{00}^{ij} \\ &= P_{11}^{ij} - P_i P_j \end{aligned} \tag{S4}$$

Due to the symmetry of the covariance ($Cov(X_i, X_j) = Cov(X_j, X_i)$), there is no loss of generality in assuming $P_i \geq P_j$. Introducing the hypothesis of hierarchical activation of the nodes (*66*) is equivalent to imposing $P_{01}^{ij} = 0$ (i.e. the less persistent node j cannot be active if the more persistent node i is dry), or $P_{11}^{ij} = P_j$. As a consequence, the covariance between the states of two nodes reads:

$$Cov(X_i, X_j) = P_j(1 - P_i)\,. \tag{S5}$$

This expression is only dependent on the persistencies of the two nodes. Let us now consider a stream network with N nodes numbered in a decreasing

order of persistency (i.e. $P_i \geq P_j$ for $i < j$). Note that node numbering does not necessarily reflect the actual position of the nodes in the physical space. The states of the nodes can be represented in a vector of random variables $\boldsymbol{X} = (X_1, X_2, ..., X_N)$. The covariance between each possible couple of nodes can be summarized in the covariance matrix, the elements of which can be expressed as:

$$Cov(\boldsymbol{X}) = \begin{cases} P_i(1-P_i) & \text{for } j = i \\ P_i(1-P_j) & \text{for } j < i \\ P_j(1-P_i) & \text{for } i > j \end{cases} \tag{S6}$$

where i and j represent the row and column indexes, respectively. At any given time, the active stream length L is a linear combination of the states of all the nodes, as per equation (S1). The stream length variance is therefore expressed as the sum of all the elements of the covariance matrix, properly weighted by the Δl_i associated to each node:

$$Var(L) = \sum_{i=1}^{N} \sum_{j=1}^{N} cov(X_i, X_j) \Delta l_i \Delta l_j \, . \tag{S7}$$

Without loss of generality, to simplify the notation a constant unit length $\Delta l_i = \Delta l = 1$ is assumed for each node. All the relevant equations, however, can be easily generalized to the case $\Delta l_i \neq const$ by properly weighting each term associated to the node i (i.e. the status X_i or the local persistency P_i) with the corresponding Δl_i. First, let us express each local persistency as the sum of the mean network persitency, $\bar{P}$, and a local deviation from the mean, ΔP_i (i.e. $P_i = \bar{P} + \Delta P_i$). Note that $\sum_{i=1}^{N} \Delta P_i = 0$ by definition. Combining equations (S6) and S7, and using the above definitions, the stream length variance can then be written as:

$$\begin{aligned} Var(L) &= \left[\sum_{i=1}^{N} P_i(1-P_i) \right] + \left[2 \sum_{i=2}^{N} \sum_{j=1}^{i-1} P_i(1-P_j) \right] \\ &= \left[N\bar{P}(1-\bar{P}) - \sum_{i=1}^{N} \Delta P_i^2 \right] + \left[(N-1)N\bar{P}(1-\bar{P}) + 2 \sum_{i=1}^{N} i \Delta P_i - 2 \sum_{i=2}^{N} \sum_{j=1}^{i-1} \Delta P_i \Delta P_j \right] \\ &= N^2 \bar{P}(1-\bar{P}) - \sum_{i=1}^{N} \Delta P_i^2 - 2 \sum_{i=2}^{N} \sum_{j=1}^{i-1} \Delta P_i \Delta P_j + 2 \sum_{i=1}^{N} i \Delta P_i \\ &\approx N^2 \bar{P}(1-\bar{P}) + N^2 \widetilde{\Delta P} \end{aligned} \tag{S8}$$

where the term $\widetilde{\Delta P} = 2/N^2 \cdot \sum_{i=1}^{N} i \Delta P_i$ represents a weighted spatial average of the persistency deviations around the mean. The weights associated to each

ΔP_i increases as i increases (i.e., as P_i decreases). Therefore, a bigger weight is attributed to the negative values of ΔP_i, and $\widetilde{\Delta P} \leq 0$. It is important to note that the last row of equation (S8) represents an approximation of the actual value of $Var(L)$, which is obtained from the full expression of $Var(L)$ by neglecting the following two terms: i) the term $\sum_{i=1}^{N} \Delta P_i^2$, that proves to be negligible when N is large (because it is of order N, while the other terms are of order N^2); ii) the term $2\sum_{i=2}^{N}\sum_{j=1}^{i-1} \Delta P_i \Delta P_j$, that is negligible because of the compensating effects originated by the interplay between the factors ΔP_i and ΔP_j when the summation indices vary. A detailed set of numerical simulations based on synthetic networks and available empirical data confirmed that the neglected terms are at least four orders of magnitude smaller then all the other terms of the equation. Equation (S8) was then combined with equation (S2) to derive equation (2) in the main paper.

Upper limits for the coefficient of variation and the standard deviation of the active drainage density

For a given stream network (i.e. a set of nodes with known local persistencies), the length variance is maximized if the activation/deactivation of the nodes follows a hierarchical order. In fact, the hierarchical activation scheme (for which $P_{01}^{ij} = 0$ if $i < j$) maximizes the joint probability that two arbitrary nodes are concurrently active ($P_{11}^{ij} = P_j$), as per equation (S3). This circumstance in turn maximizes the covariance of the states of each couple of nodes in the network (equation (S5)) and the active length variance (as per equation (S7)).

Furthermore, a stream network in which all the nodes share the same persistency originate an higher active length variance with respect to any other possible network with the same mean network persistency $\bar{P}$. Intuitively, this property is directly implied by the hierarchical activation scheme, according to which all the nodes are activated or deactivated at the same time as long as they share the same persistency. In such a case, the active length can only assume the limiting values of 0 and L_g, thereby ensuring the maximization of the temporal variance of the active length. The same conclusion can be obtained analyzing the term $\widetilde{\Delta P} \leq 0$ in equation (S8). $\widetilde{\Delta P}$, in fact, is a weighted spatial average of the fluctuations of persistency around the mean. In the case where all nodes share the same persistency, $\Delta P_i = 0$ for each i, and $\widetilde{\Delta P} = 0$, allowing the maximization of the length variance (as per equation (S8)). Based on equation (S8), the upper limit for the variance of the active stream length can be written as:

$$Var^{max}(L) \approx N^2 \bar{P}(1-\bar{P}) \tag{S9}$$

This equation can be easily combined with equation (S2) to obtain equation (3) in the main paper. Equation (S9) shows that the universal maximum variance of the active length is obtained when $\bar{P} = 0.5$, because under these circumstances the term $\bar{P}(1-\bar{P})$ is maximized. In such a case, $Var^{max}(L) = 0.25N^2$, where N is the geomorphic length due to the assumption that $\Delta l_i = \Delta l = 1$.

The universal upper bound of the length standard deviation is then:

$$dev(L) = \left[Var^{max}(L)\right]^{0.5} = 0.5L_g \tag{S10}$$

as reported in the main text.

Coefficient of variation of the drainage density for beta-distributed persistencies

The available empirical data show that the frequency distribution of the local persistency of the different nodes in the network, here denoted as $pdf(P)$, can be reasonably described by a Beta distribution with the first shape parameter set to 1:

$$pdf(P) = \frac{(1-P)^{\beta-1}}{B(1,\beta)} \, . \tag{S11}$$

In the above equation P is the local persistency, β is the second shape parameter of the distribution and $B(1,\beta) = \frac{1}{\beta}$. For each case study, the parameter β was calculated using the method of moments based on the mean network persistency, $\bar{P}$. In particular, the analytical expression of the first moment of the Beta distribution was exploited to calculate the free shape parameter as a function of the mean network persistency:

$$\beta = \frac{1-\bar{P}}{\bar{P}} \, . \tag{S12}$$

The analogous expression for the second-order moment of the Beta distribution can be used to evaluate the spatial variance of the local persistency as:

$$Var(P) = \frac{\bar{P}^2(1-\bar{P})}{1+\bar{P}} \tag{S13}$$

Likewise, $\widetilde{\Delta P}$ can be expressed as follows:

$$\widetilde{\Delta P} = -\frac{\bar{P}(1-\bar{P})}{2-\bar{P}} \tag{S14}$$

Equations (S8) and (S14) were then combined to obtain the following expression of the variance of the active length when the local persistencies are beta-distributed:

$$Var(L) = N^2 \frac{\bar{P}(1-\bar{P})^2}{1-\bar{P}} \tag{S15}$$

Equation (4) of the main paper is then derived combining equations (S2) and (S15).

1.9 Monitoring hierarchical networks

If the activation and deactivation of the nodes of a dynamic stream network obeys to a purely hierarchical scheme, the monitoring of active stream length dynamics can be significantly facilitated. In fact, the hierarchical assumption can be used to deduce the status of some nodes in the network from the observed status of other nodes. Specifically, if a node is observed as wet then all the nodes in the network with a larger persistency should be wet. Likewise, if a node is dry, then all the nodes with a smaller persistency should be dry as well. One might argue that prior to the field campaign for the monitoring of active stream network dynamics the persistencies of the nodes are not known. However, as long as the surveys take place, this hierarchy is progressively revealed and, crucially, the hierarchies emerging during any survey will remain unchanged for the entire campaign. Thus, as the number of available active stream network maps increases, the ability to extrapolate in space information about the status of the nodes increases as well. To quantify the number of nodes that do not need to be visited during a field campaign (because their status can be deduced from the status of other nodes), a series of numerical simulations was performed in which we simulated the dynamics of the stream network by simulating a hierarchical chain of nodes and the position of the transition between wet and dry nodes in the chain. Likewise, the number of nodes that has to be visited using the information available prior to the survey is computed. These numerical simulations consisted in the following steps: i) a sequence of N nodes with a dichotomic status and a fixed distribution of the local persistencies is considered; ii) the nodes are first re-ordered in a chain following a decreasing order of local persistency (the first node is the most persistent, the last node the least persistent); iii) an auxiliary counting variable, k, is set equal to 1; iii) the position of the unique transition between wet and dry nodes in the chain is identified by selecting randomly one of the existing groups of nodes in the chain; if $k = 1$ the position of the transition is set within the unique group containing all the N nodes of the chain; iv) the selected group is then randomly split into two sub groups (namely, the group of wet nodes and the group of dry nodes) and a new group is thus created; v) a new hierarchy is created between these two node subgroups by assigning an apparent persistency P_a to the existing $k+1$ groups as follows: $P_a = s/k$, where s is the number of times that a group of nodes was observed as active during the campaign up to the k^{th} survey; vi) the number of nodes to be visited during the k^{th} survey to characterize the whole active network is then computed as the sum of the number of nodes that need to be surveyed to identify the groups within which the transition takes place (i.e., the number of existing groups k) plus the number of nodes that need to be visited to identify the precise location of that transition within the nodes of the relevant groups (all the nodes that are included in the two groups where the transition takes place); vii) the counting variable k is increased to the subsequent integer number and the procedure starts again from step iii). The procedure stops when a pre-determined number of field surveys (say, K) is performed. The percentage of nodes that has to be surveyed is then calculated as the number of surveyed

nodes during the whole campaign scaled to the number of nodes that potentially have to be visited (i.e., $N\,K$). The simulations were performed with different combinations of K, N and $\bar{P}$, and the results are shown in Figure S8. The plot indicates that, for hierarchical networks, the number of nodes to be visited is between 60 to 30 % of the overall number of nodes that should be surveyed in non-hierarchal networks, with smaller percentages associated to field campaigns made up of a larger number of surveys.

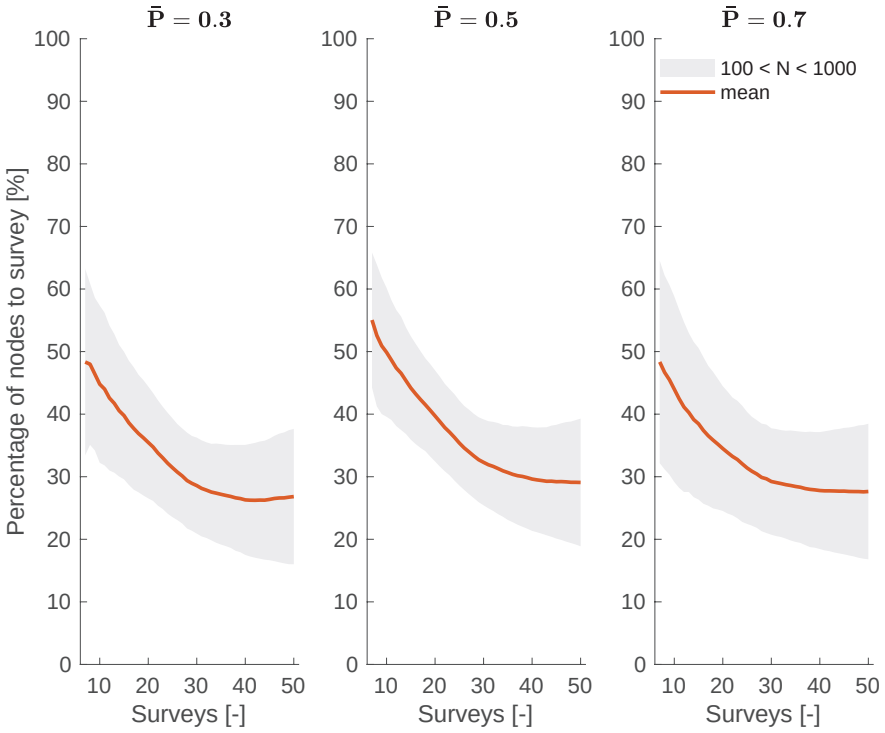

Figure S8: Percentage of nodes to survey in perfectly hierarchical networks, as a function of the number of performed surveys and the number of nodes, N. The orange line shows the average, while the shadowed area shows the range obtained by varying the number of nodes in the network between 100 and 1000.

References

58. L. Pfister, N. Martìnez-Carreras, C. Hissler, J. Klaus, G. E. Carrer, M. K. Stewart, and J. J. McDonnell, "Bedrock geology controls on catchment storage, mixing, and release: a comparative analysis of 16 nested catchments," *Hydrological Processes*, vol. 31, pp. 1828–1845, 2017.

59. O. national des étiages, "Onde dataset," 2020. Fata retrieved from https://onde.eaufrance.fr/.

60. "Hubbard brook experimental forest: Total daily precipitation by watershed, 1956 - present." Available at https://doi.org/10.6073/pasta/c64ad38eef4f56d9e34749f166f64caa.

61. P. J. Edwards and F. Wood, "Fernow experimental forest daily precipitation." Available at https://doi.org/10.2737/RDS-2011-0014.

62. C. F. Miniat, S. H. Laseter, W. T. Swank, and L. W. J. Swift, "Daily precipitation data from recording rain gages (rrg) at coweeta hydrologic lab, north carolina." Available at https://doi.org/10.2737/RDS-2017-0031.

63. "Usgs monthly et data." https://earlywarning.usgs.gov/ssebop/modis/8-day/607.

64. G. Senay, "Satellite psychrometric formulation of the operational simplified surface energy balance (SSEBop) model for quantifying and mapping evapotranspiration," *Applied Engineering in Agricolture*, vol. 34, pp. 555–566, 2018.

65. R. Allen, M. Smith, W. Pruitt, and L. Pereira, "Modification of the FAO crop coefficient approach," *Proceedings of the International Conference*, pp. 124–132, 1996.

66. G. Botter and N. Durighetto, "The stream length duration curve: a tool for characterizing the time variability of the flowing stream length," *Water Resources Research*, vol. 56, 2020.